THE ASTROPHYSICAL JOURNAL, 567:672–701, 2002 March 10

CALTECH FAINT GALAXY REDSHIFT SURVEY. XVI. THE LUMINOSITY FUNCTION FOR GALAXIES IN THE REGION OF THE HUBBLE DEEP FIELD–NORTH TO $z = 1.5$[1]

JUDITH G. COHEN[2]

Received 2001 July 5; accepted 2001 October 22

ABSTRACT

We have carried out a study of the luminosity function (LF) of galaxies in the region of the Hubble Deep Field–North using our very complete redshift catalog. We divide the sample into five redshift bins covering the range $0.01 < z < 1.5$ and consider three primary galaxy spectral classes. We solve for the LF at four rest-frame wavelengths from 0.24 to 2.2 μm. We find that the LFs for quiescent galaxies have shallow faint-end slopes while those of galaxies with detectable emission lines have steeper faint-end slopes. Furthermore, these slopes appear to be independent of redshift out to $z = 1.05$ for each galaxy spectral grouping and agree well with comparable local determinations. We then fix α to obtain values of L^* for each galaxy spectral grouping as a function of redshift. We find that galaxies with strong absorption lines become brighter with z with $Q \sim 0.6$ at all rest-frame bands studied here, where $Q = \Delta \log [L^*(z)]/\Delta z$, while galaxies with detectable emission lines (i.e., star-forming galaxies) show a smaller change in L^* with redshift at all bands, $Q \sim 0.3$, with Q becoming significantly larger at rest-frame 2400 Å. Passive evolution models of galaxies are in reasonable agreement with these results for absorption-line–dominated galaxies, while plausible star formation histories can reproduce the behavior of the emission-line galaxies. We find a constant comoving number density and stellar mass in galaxies out to $z \sim 1.05$. By stretching all the correction factors applied to the galaxy counts in the highest redshift bin to their maximum possible values, we can just barely achieve this between $z = 1.05$ and 1.3. The major epoch(s) of star formation and of galaxy formation must have occurred even earlier. The UV luminosity density, an indicator of the star formation rate, has increased by a factor of $\sim$4 over the period $z = 0$–1.

Subject headings: cosmology: observations — galaxies: fundamental parameters — galaxies: luminosity function, mass function — galaxies: stellar content — surveys

On-line material: machine-readable table

1. INTRODUCTION

The goal of the Caltech Faint Galaxy Redshift Survey (CFGRS) is to understand the evolution of galaxies to $z \gtrsim 1$. In this paper we present the luminosity function (LF) for galaxies in the region of the Hubble Deep Field–North (HDF-N) (Williams et al. 1996) from our very complete redshift survey.

First we discuss the completeness of the observed sample in U, R, and K. We describe the derivation of the rest-frame LF in R in some detail in § 3. We then briefly indicate the differences in procedure for rest-frame 2400 Å, U, and K. We discuss the evolution with redshift of L^* (the characteristic luminosity of the LF), the comoving number density, and the comoving luminosity density for various galaxy spectral groupings from $z = 0.01$ to 1.5. We then compare our results to Poggianti's (1997) models for galaxy spectral evolution in § 9. In § 9.1 we compute the total stellar mass in galaxies as a function of redshift. Comparisons with the results obtained by previous redshift surveys are given in § 11.

Throughout, our goal, given the sample size in hand, is the simplest possible analysis, even if at some sacrifice of accuracy, since errors arising from the small sample size will dominate over any limitations imposed here through use of a relatively unsophisticated analysis. Appendix B demonstrates that the derived luminosity densities are very robust.

As in earlier papers in this series, we adopt the cosmology $H_0 = 60$ km s^{-1} Mpc^{-1}, $\Omega_M = 0.3$, $\Omega_\Lambda = 0$. Over the redshift interval of most interest, a flat universe with $\Omega_\Lambda = 0.7$ and a Hubble constant of $H_0 = 67$ km s^{-1} Mpc^{-1} gives galaxy luminosities very close to those derived below. Additional comments regarding modifying the adopted cosmology are given in § 10.

We use luminosities rather than magnitudes. By luminosity, we mean the quantity νL_ν with units of W at a particular wavelength in the rest frame. We express luminosities as the base-10 logarithm of this quantity. See Cohen et al. (2000, hereafter C00) for more details.

2. THE SAMPLE

The redshift survey of galaxies in the region of the HDF by C00, supplemented in Cohen (2001), is the sample used here. This survey strives for a complete set of redshifts for all objects with $R < 24.0$ in the HDF itself and for objects with $R < 23.5$ in the Flanking Fields within a diameter of 8′ centered on the HDF. Extremely high completeness (95% for the HDF and $\gtrsim$93% for the Flanking Fields) was achieved through a spectroscopic program that extended over 5 yr.

The primary source of photometry is Hogg et al. (2000, hereafter H00), who present four color catalogs for galaxies in the region of the HDF. They used the SExtractor package (Bertin & Arnouts 1996) and relied on it to extrapolate the measured magnitudes to a large aperture.

[1] Based in large part on observations obtained at the W. M. Keck Observatory, which is operated jointly by the California Institute of Technology, the University of California, and NASA.

[2] Palomar Observatory, Mail Stop 105-24, California Institute of Technology, Pasadena, CA 91125.

The spectral energy distributions (SEDs) of these galaxies were derived, parameterized in the rest frame, by Cohen (2001). Those fits are adopted to calculate all luminosities used in this paper. SED parameters for six galaxies in the Flanking Fields with redshifts taken from Dawson et al. (2001) are given in Appendix A.

At least for the HDF itself, the issue of possibly missing low surface brightness galaxies is moot in the redshift range under consideration here since the *Hubble Space Telescope* (*HST*) WFPC2 imaging of Williams et al. (1996) is extremely deep with respect to the limiting magnitude of the redshift survey (see also Driver 2001). We assume that the H00 photometric catalog in the Flanking Fields is not seriously affected by the potential loss of low surface brightness galaxies.

Our redshift catalog for the region of the HDF contains 735 objects, of which 631 are galaxies with $0 < z < 1.5$. A total of 10 galaxies (all with $0.25 < z < 1.5$) are located just outside the 8′ diameter sample boundary and are excluded. The two active galactic nuclei (AGNs) with $z < 1.5$ are also excluded from the sample used for the LF analysis.

We use the galaxy spectral classification scheme defined in Cohen et al. (1999), which basically characterizes the strength of the strongest emission lines, particularly [O II] at 3727 Å, [O III] at 5007 Å, and Hα, relative to the strong absorption features, H and K of Ca II and the normal absorption in the Balmer lines. To review briefly, "$\mathscr{E}$" galaxies have spectra dominated by emission lines, "$\mathscr{A}$" galaxies have spectra dominated by absorption lines, and "$\mathscr{I}$" galaxies are of intermediate type. Galaxies with broad emission lines are denoted as spectral class "$\mathscr{2}$." Starburst galaxies showing the higher Balmer lines (Hγ, Hδ, etc.) in emission are denoted by "$\mathscr{B}$," but for such faint objects it was not always possible to distinguish them from "$\mathscr{E}$" galaxies. These classifications were assigned for the galaxies in our sample in the region of the HDF in C00 (see also Cohen 2001).

While the galaxy spectral classes that we use are very broad, the possibility remains that galaxies may evolve between them over time. We must draw a distinction between evolution of the LF with redshift and evolution of a particular galaxy with time.

2.1. *Completeness at Observed U, R, and K Bands*

The calculation of completeness for our redshift survey in the region of the HDF at observed R is straightforward as the sample for our redshift survey was selected from the very deep R-band photometric catalog of H00. We evaluate the completeness at R by matching the redshift catalog and the R-band photometric catalog of H00. This was done in C00 but has to be reevaluated here as additional redshifts, primarily from Cohen (2001), further increase the completeness. We require not the cumulative completeness, but the completeness of the redshift survey per bin in R magnitude, $C(R)$, which we determine in 0.25 mag bins. While the former is very high, the completeness per magnitude bin is falling fairly rapidly at the faintest bins.

We cut off the sample for calculating the LF where the completeness in a 0.25 mag bin falls to $\sim$40% for the Flanking Fields, which occurs at $R = 23.5$, and cut at $R = 24$ for the HDF itself. Of the 631 galaxies with $0.01 < z < 1.5$, 12 in the HDF have $R > 24$, and 50 in the Flanking Fields have $R > 23.5$. This leaves a total sample of 553 galaxies.

Thus, the sample actually analyzed here for the LF at rest-frame R consists of 553 galaxies with $0.01 < z < 1.5$, 93 of which are in the HDF and 460 of which are in the Flanking Fields. There are 21 galaxies in the HDF with $23.5 < R < 24$, between the limits of the Flanking Fields cutoff in R and that of the HDF itself.

The photometric catalog of H00 is not sufficiently deep at observed K or U. A study of the counts for the H00 catalog as a function of magnitude suggests that it becomes significantly incomplete at $U > 24.5$ and $K > 20.5$. Hence, there are many objects in the redshift catalog with no detection at K in the H00 database. For objects missing K and U photometry in H00, we therefore augment this primary photometric database by adding photometry at K and U from the unpublished catalog of Barger, described in Barger et al. (1999). If there is still no observation at K, we assume $R-K = 3.1$, the median value for the sample at $z > 0.5$. If there is still no observation at U, we use $U-R = 1.1$ mag, again the median for the sample at $z > 0.5$, except for $\mathscr{A}$ galaxies, where we assume $U-R = 5.0$ mag. There are only 24 galaxies in the redshift sample with $0.01 < z < 1.5$ for which U is missing, many of which either are close pairs or represent matching problems between the various catalogs. The completeness for the Flanking Fields is then calculated in the same way described above as was used for R.

For the HDF itself, we augment the H00 photometric database with photometry from the Hawaii group and then use the catalog of Fernandez-Soto, Lanzetta, & Yahil (1999) as the master list against which the completeness is evaluated for $K > 20$. For brighter magnitudes, the H00 photometric catalogs as supplemented with the Hawaii catalogs are used.

The resulting values for the HDF and for the Flanking Fields are listed in Table 1. All objects in this field brighter than the brightest entry in the table are Galactic stars.

The values used to calculate weights for the LF analysis are slightly smoothed from those given in the table. The observed K completeness corrections were used for the rest-

TABLE 1

COMPLETENESS AT OBSERVED U, R, AND K

Magnitude Range	N(Phot)(HDF)	%(z)(HDF)	N(Phot)(FF)	%(z)(FF)
		Observation U		
17.00–17.25	0	...	2	100
17.25–17.50	0	...	0	...
17.50–17.75	0	...	1	...
17.75–18.00	0	...	1	...

NOTE.—Table 1 is published in its entirety in the electronic edition of the *Astrophysical Journal*. A portion is shown here for guidance regarding its form and content.

frame K analysis, the observed R completeness corrections were used for the rest-frame R and U analysis, and the observed U completeness corrections were used for the analysis at rest-frame 2400 Å.

2.2. *The Two Weighting Schemes Used*

Two weighting schemes are applied in the following LF analysis. The first is the conventional weighting scheme used by many previous such analyses, $W[G(R, z)] = 1/C(R)$, where $G(R, z)$ denotes a sample galaxy with redshift z and observed R magnitude. Here the weight is a reflection of the completeness at a given magnitude of the redshift catalog. The general practice is to assign the missing galaxies (i.e., the weight in excess of unity) to the redshift of the observed galaxy. We refer to this scheme as the "R magnitude weights." Similar weights have been calculated for K and for U.

In addition, because of the difference in magnitude cutoff between the HDF and the Flanking Fields, we multiply the weight of those objects in the HDF with $23.5 < R < 24$ by the ratio of the solid angle subtended by the Flanking Fields to that of the HDF itself, which is 9.47.

These weights are valid if, and only if, the probability of determining a redshift is a function only of magnitude. However, in our sample the range of redshift is very large. The technical difficulties associated with the "redshift desert," the regime $1.2 \lesssim z \lesssim 2$, between where the standard optical emission lines shift out of the optical band and the strong UV lines and Lyman limit move in, make redshift determinations in this z regime extremely difficult. The weighting scheme used ideally should take this into account.

Hence, we introduce a second set of weights which we call the high-z weights. The number of objects that should be included in the sample based on their photometry but that are without redshifts is computed as before. However, *all* the missing objects are put into the highest redshift bin. Obviously use of the high-z weights would be unacceptable in a sample with low completeness and with many bright (and hence presumably "nearby") objects without redshifts, but with the present sample we view it as a only a moderate extrapolation from reality.

3. THE ANALYSIS PROCEDURE

We emphasize that the galaxy SEDs are specified in the rest frame (see Cohen 2001) and that all LFs are evaluated in the rest frame. We begin with rest-frame R, as the completeness corrections in the observed R band are very accurately known to faint magnitudes as a result of the depth of the photometry catalog of H00 and the SEDs are very well defined there as well. Note that $M_R = -22.00$(restframe) $\equiv$ log $[L(R)(W)] = 36.97$. No extinction corrections for gas or dust within the galaxies themselves have been applied.

3.1. *The Two-Parameter Schechter Fits*

We use a standard maximum likelihood technique to compute the LFs (Sandage, Tammann, & Yahil 1979; Efstathiou, Ellis, & Peterson 1988; Lin et al. 1999). We assume that a Schechter (1976) function adequately describes the LF at each z for each set of galaxy spectral classes considered. The R magnitude range is from 16 (there is nothing brighter in this field except Galactic stars) to the faint-end cutoff (24 in the HDF, 23.5 in the Flanking Fields). As a first reconnaissance of the problem, we break the sample into the same four redshift ranges over the regime from $z = 0.25$ to 1.5 adopted in Cohen (2001). We add when feasible (i.e., for the rest-frame U, R, and K bands) the regime $0.01 < z < 0.25$ with some trepidation due to the selection of the HDF as a field devoid of bright galaxies (Williams et al. 1996) as well as the limited volume at low redshift of the narrow pencil beam probed here.

Table 2 lists the mean redshift of each of the five bins as defined by the galaxies in the redshift sample as well as the comoving volume of the bins. The mean redshift of the observed sample is biased high for the low-redshift bins, where the increase in available volume is more rapid than the drop-off due to increasing distance and decreasing apparent brightness. It is biased somewhat low in the high-redshift bins, where the volume is increasing slowly while the apparent brightness is dropping steadily. The mean redshift of the bins is also slightly affected by the presence and exact redshifts of the most populous galaxy groups within some of the bins. In accordance with our philosophy of simplicity in the analysis described above, we ignore clustering. C00 have shown that while there are no clusters (i.e., nothing comparable to an Abell cluster) in this sample, there are many populous groups of galaxies.

We carry out a standard two-parameter solution for the characteristic luminosity L^* and for the faint-end slope α for the Schechter function $\phi(L) = dN/dL = \phi^* e^{-L/L^*}(L/L^*)^{\alpha}$. We are thus assuming that within each of the bins, these two parameters can be taken as roughly constant. The details of the analysis are similar to that described by Lin et al. (1999). We have five redshift bins, and we use six groupings of galaxy spectral classes. The first three are the primary galaxy spectral classes, $\mathscr{A}$, $\mathscr{I}$, and $\mathscr{E} + \mathscr{B}$ (hereafter just denoted as $\mathscr{E}$). We also introduce two groupings of spectral classes to try to take into account the probable migration of galaxies between spectral classes due purely to technical difficulties, $\mathscr{A} + \mathscr{I}$ and $\mathscr{I} + \mathscr{E}$, as well as the class containing all galaxies (excluding AGNs).

We require a minimum sample of 15 galaxies in a bin. The $\mathscr{I}$ galaxy sample in the bin $0.8 < z < 1.05$ is too small in the R-selected sample to be analyzed independently. This is probably not an indication of a decline in the number of such galaxies but rather of a decline in our ability to discriminate between $\mathscr{I}$ galaxies and $\mathscr{E}$ galaxies with spectra of a fixed exposure time and hence limited signal-to-noise ratio. The sample in the lowest redshift bin is very small and can only be analyzed as a whole, as is also true of the highest redshift bin.

There are several additional issues that affect the highest redshift bin. First, the spectral types there are not comparable in their meaning to those for galaxies with $z < 1$. Specifically, galaxy spectral class $\mathscr{A}$ in the $z < 1$ sample refers to

TABLE 2

PROPERTIES OF THE REDSHIFT BINS

z Range	Mean z	Comoving Volume (Mpc^3)
0.01–0.25.....	0.15	39
0.25–0.5	0.41	183
0.5–0.8	0.60	429
0.8–1.05	0.90	487
1.05–1.5	1.22	1206

galaxies with strong Ca II H and K lines, obvious Balmer line absorption, and a strong 4000 Å break. At $z > 1.1$, however, this galaxy spectral class designates the presence of absorption features and breaks characteristic of the 2500 Å mid-UV. This is not an issue in the present work as the sample there is too small to subset in any way.

For the highest redshift bin, where the sample is dominated by galaxies with strong emission lines, the range of $L(R)$ probed by our sample is small. Hence, the stability of the full solution is delicate. In the local universe, samples of such galaxies show a very steep faint-end slope. The solution for such an LF is much more difficult than for one with the more modest faint-end slope seen in the local universe for $\mathscr{A}$ galaxies. There the LF has a well-defined bend that can be used to separate α and L^*. Such a characteristic break is absent in local samples (and, as we will see, the present high-redshift samples as well) of $\mathscr{E}$ galaxies, making the separation of α and L^* much more difficult.

If we consider the small sample in the highest redshift bin, the fluctuations introduced by a few extra galaxies in the HDF with $23.5 < R < 24.0$ are unacceptably large because the weight of each such galaxy in this gray zone is high (≥ 9.4). In a large sample, this can be tolerated, but in this bin with $1.05 < z < 1.5$ the total sample is very small, and the excess weight of the $\sim 25\%$ of the galaxies in the gray zone introduces an instability. The solution slides toward very high values of L^* and very steep faint-end slopes, even though no galaxies so luminous as the putative L^* or anything near it actually exist in the sample. To overcome this, we found that the best way to proceed was, for the highest redshift bin only, to cut the sample back to limits of $R = 23.5$ in the HDF as well as in the Flanking Fields, thus making the cutoff the same over the entire area of the survey. A similar restriction of the maximum allowed weight had to be imposed in all rest-frame bands attempted for the highest redshift bin only.

In the case of the highest redshift bin, although there are 38 galaxies in our redshift catalog for the region of the HDF with $1.05 < z < 1.5$, seven of them have $R > 24.0$ and thus are excluded from the R-selected sample irrespective of location. Six more are located in the Flanking Fields with $R > 23.5$ and hence are eliminated. Six more are in the HDF with $23.5 < R < 24.0$ and also had to be eliminated from the R-selected sample.

The results of this classical analysis are given in Table 3 for the six galaxy spectral class groupings. The errors given in this table and in Table 4 are 1 σ uncertainties for one parameter. The error is measured by projecting along the relevant axis the full range of the two-dimensional error contours. These, for a fixed number of objects, depend on the shape of the two-dimensional uncertainty contours, which are shown in Figures 1–6. The 90% confidence level

TABLE 3

SOLUTIONS FOR $L^*(R)$ AND α

z Range	Total Number	Number in HDF	Number in Flanking Fields	log [$L^*(R)$] (W)	α
			$\mathscr{A}$ Galaxies		
0.25–0.5	17	1	16	37.15 ± 0.45	-0.73 ± 0.60
0.5–0.8	36	6	30	37.19 ± 0.30	-0.43 ± 0.50
0.8–1.05	19	7	12	37.32 ± 0.50	-0.40 ± 1.00
			$\mathscr{I}$ Galaxies		
0.25–0.5	62	7	55	36.73 ± 0.25	-0.19 ± 0.40
0.5–0.8	63	8	55	36.85 ± 0.25	0.08 ± 0.55
0.8–1.05	14	2	12	...	...
			$\mathscr{A} + \mathscr{I}$ Galaxies		
0.25–0.5	79	8	71	36.83 ± 0.25	-0.35 ± 0.35
0.5–0.8	99	14	85	37.00 ± 0.20	-0.19 ± 0.40
0.8–1.05	33	9	24	37.16 ± 0.45	0.11 ± 1.00
			$\mathscr{I} + \mathscr{E}$ Galaxies		
0.25–0.5	131	23	108	37.00 ± 0.35	-1.07 ± 0.20
0.5–0.8	164	23	141	37.39 ± 0.35	-1.39 ± 0.20
0.8–1.05	125	18	107	37.20 ± 0.25	-1.19 ± 0.40
			$\mathscr{E}$ Galaxies		
0.25–0.5	69	16	53	36.75 ± 0.40	-1.50 ± 0.25
0.5–0.8	101	15	86	37.19 ± 0.45	-1.71 ± 0.25
0.8–1.05	111	16	95	37.05 ± 0.20	-1.09 ± 0.60
			All Galaxies		
0.01–0.25.....	37	6	31	$>36.70 \pm 0.60$[a]	-1.06 ± 0.25
0.25–0.5	148	24	124	37.13 ± 0.25	-1.08 ± 0.15
0.5–0.8	200	29	171	37.47 ± 0.25	-1.28 ± 0.25
0.8–1.05	144	25	119	37.37 ± 0.25	-1.28 ± 0.30
1.05–1.50.....	18[b]	4	14	37.30 ± 0.40	-0.45 ± 1.30

[a] Assigned as a lower limit as a result of selection criteria for HDF.

[b] Six galaxies in the HDF with $23.5 \leq R \leq 24.0$ had to be eliminated. See text for details.

TABLE 4

SOLUTIONS FOR $L^*(K)$ AND α

z Range	Total Number	Number in HDF	Number in Flanking Fields	log [$L^*(K)$] (W)	α
			$\mathscr{A}$ Galaxies		
0.25–0.5	15	0	15	37.00 ± 0.50[a]	-0.57 ± 0.40[a]
0.5–0.8	36	6	30	36.90 ± 0.25	0.07 ± 0.40
0.8–1.05	19	7	12	37.15 ± 0.45	-0.07 ± 0.70
			$\mathscr{I}$ Galaxies		
0.25–0.5	60	7	53	36.75 ± 0.25	-0.60 ± 0.25
0.5–0.8	62	7	55	36.70 ± 0.25	-0.21 ± 0.40
0.8–1.05	16	2	14	36.70 ± 0.50	1.20 ± 1.20
			$\mathscr{A} + \mathscr{I}$ Galaxies		
0.25–0.5	75	7	68	36.80 ± 0.25	-0.60 ± 0.25
0.5–0.8	98	13	85	36.85 ± 0.20	-0.21 ± 0.30
0.8–1.05	35	9	26	37.00 ± 0.30	0.22 ± 0.60
			$\mathscr{I} + \mathscr{E}$ Galaxies		
0.25–0.5	115	22	93	37.10 ± 0.40	-1.25 ± 0.10
0.5–0.8	147	17	130	37.00 ± 0.25	-1.23 ± 0.20
0.8–1.05	121	15	106	37.10 ± 0.30	-1.13 ± 0.30
			$\mathscr{E}$ Galaxies		
0.25–0.5	55	15	40	37.00 ± 0.60	-1.68 ± 0.20
0.5–0.8	85	10	75	36.40 ± 0.40	-1.26 ± 0.35
0.8–1.05	105	13	92	37.00 ± 0.35	-1.20 ± 0.30
			All Galaxies		
0.01–0.25.....	30	5	25	$>36.40 \pm 0.40$[b]	-0.81 ± 0.15
0.25–0.5	130	22	108	37.10 ± 0.30	-1.21 ± 0.15
0.5–0.8	183	23	160	37.20 ± 0.25	-1.16 ± 0.15
0.8–1.05	140	22	118	37.30 ± 0.30	-1.14 ± 0.25
1.05–1.50	27[c]	10	17	37.25 ± 0.40	-1.04 ± 0.70

[a] These are 1 σ one-parameter errors throughout. See Figs. 1–6 for the two-parameter error contours.
[b] Assigned as a lower limit as a result of selection criteria for HDF.
[c] One galaxy in the HDF with weight greater than 15 had to be eliminated. See text for details.

contours are indicated in these figures calculated in accordance with § 14.5 of Press et al. (1986) for each of the galaxy spectral groupings for the three bins between $z = 0.25$ and 1.05.

Efstathiou et al. (1988) evaluated the expected variance of α and L^* analytically as a function of sample size and verified their predictions with Monte Carlo calculations. Using their formulae, we expect $\sigma(\alpha) = 0.25$ for a sample of 100 galaxies. Our measured errors are in reasonable agreement with their formulae.

Figures 7 and 8 show the resulting LF for two galaxy spectral groupings ($\mathscr{A} + \mathscr{I}$ and $\mathscr{E}$) for the redshift bin $0.5 < z < 0.8$. The best-fit LF from Table 5 is also shown superposed on the data. The lower panels in each of these figures show the errors in the LF due to Poisson statistics as a function of luminosity for these two cases. The number of galaxies per step in log L is largest in the region just below L^*. Brighter than that, the factor of e^{-L/L^*} rapidly cuts the observed galaxy numbers in a small sample such as ours to zero, while within a fixed redshift interval the faint-end magnitude cutoff of the redshift survey truncates the faint end of the luminosity distribution of the observed galaxies. When there is only one galaxy in a bin, $\Delta(\phi)/\phi$ becomes unity.

4. THE LF AT REST-FRAME U, K, AND 2400 Å

Because of the substantial mean redshift of the sample, the calculations for the LF parameters at rest-frame U are made using the observed R-selected sample and use the observed R weights, as do those at rest-frame R. Hence, they are quite similar to those for rest-frame R described above. The same treatment of the highest redshift bin was required, eliminating all galaxies with $23.5 < R < 24$ in the HDF. The LF parameters for rest-frame U are given in Tables 6 and 7, as well as interspersed in subsequent tables.

The calculations at rest-frame K used the observed K-selected sample and the observed K weights. The number of galaxies in a redshift bin used to determine the LF at rest-frame K depends on the faint-end cutoffs adopted for observed K and on the color of each galaxy and hence often will not be exactly the same as used for the R-selected LF but should be fairly close. Some of the bluer and fainter among the $\mathscr{E}$ galaxies which are members of the R-selected sample may be too faint to be included in the K-selected sample. In addition, since the observations for the redshift catalog were defined by an observed R photometric catalog, there will be a more gradual decline in completeness near the survey limit at any other observed band as a result of the range of colors of galaxies.

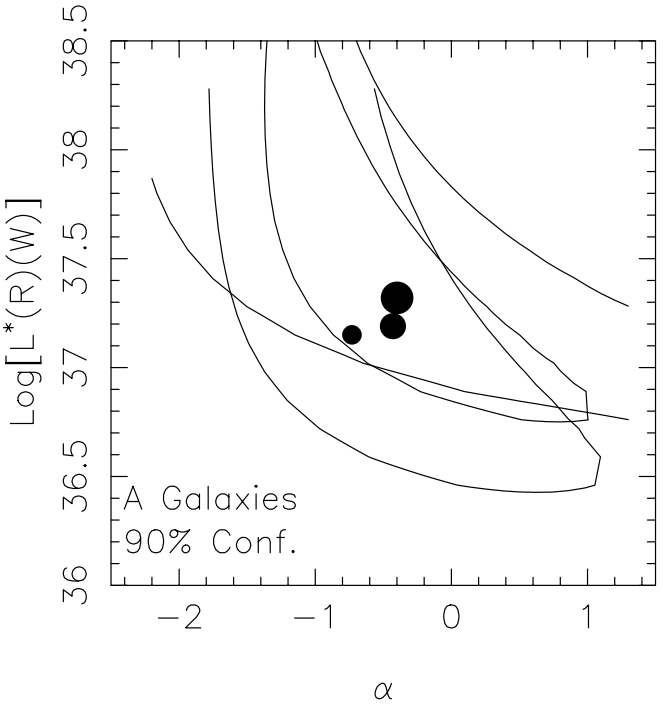

FIG. 1.—90% confidence level contours for α and $L^*(R)$ for the $\mathscr{A}$ galaxies shown for the three redshift bins between $z = 0.25$ and 1.05. The filled circle, whose size increases with increasing redshift of the bin, denotes the maximum likelihood solution.

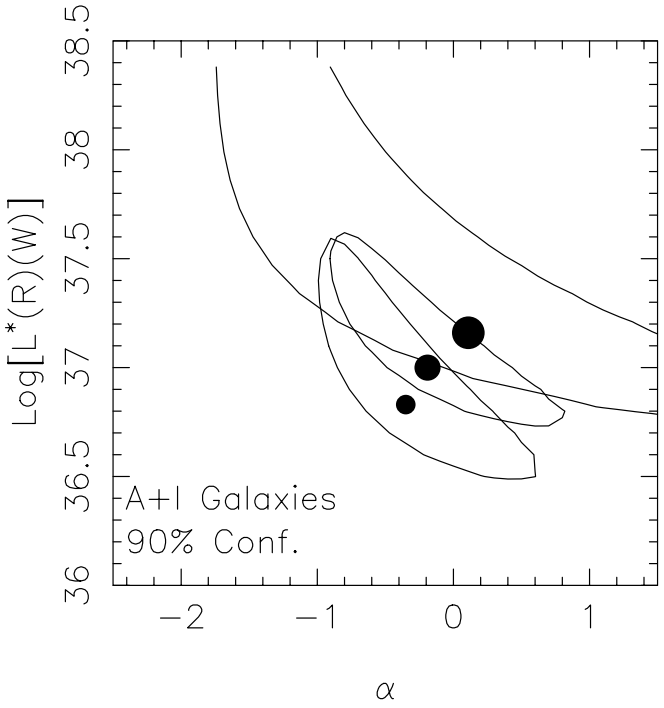

FIG. 3.—90% confidence level contours for α and $L^*(R)$ for the $\mathscr{A} + \mathscr{I}$ galaxies shown for the three redshift bins between $z = 0.25$ and 1.05. The filled circle, whose size increases with increasing redshift of the bin, denotes the maximum likelihood solution.

For the LF at rest-frame K, we proceed as with the R-selected sample. We adopt a faint-end cutoff for observed K of 20.75 in the Flanking Fields and 21.25 in the HDF. To obtain convergence in the highest redshift bin, we had to establish a maximum weight of 15, thus eliminating a small number of galaxies. With this modification, the highest z bin converged well with a total of 27 galaxies included with $1.05 < z < 1.5$.

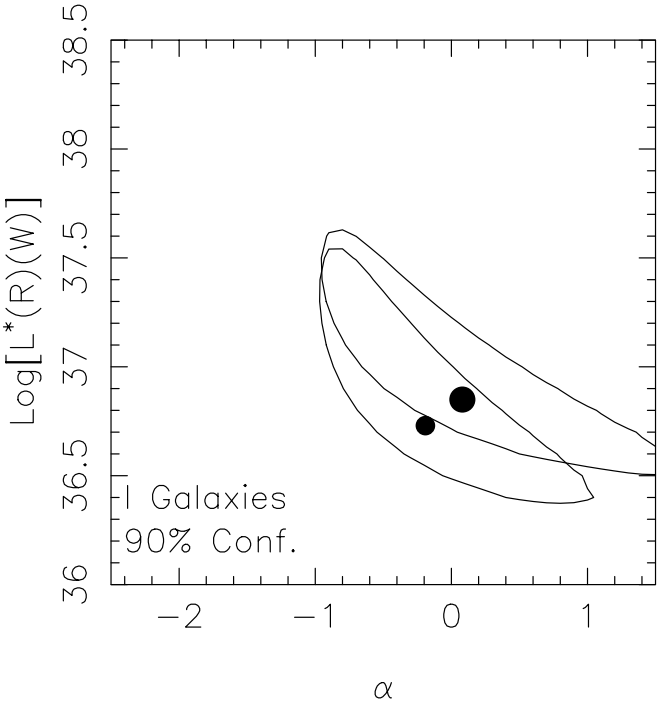

FIG. 2.—90% confidence level contours for α and $L^*(R)$ for the $\mathscr{I}$ galaxies shown for the redshift bins $0.25 < z < 0.50$ and $0.50 < z < 0.80$ only. (The sample in this galaxy spectral grouping is too small in the higher redshift bins.) The filled circle, whose size increases with increasing redshift of the bin, denotes the maximum likelihood solution.

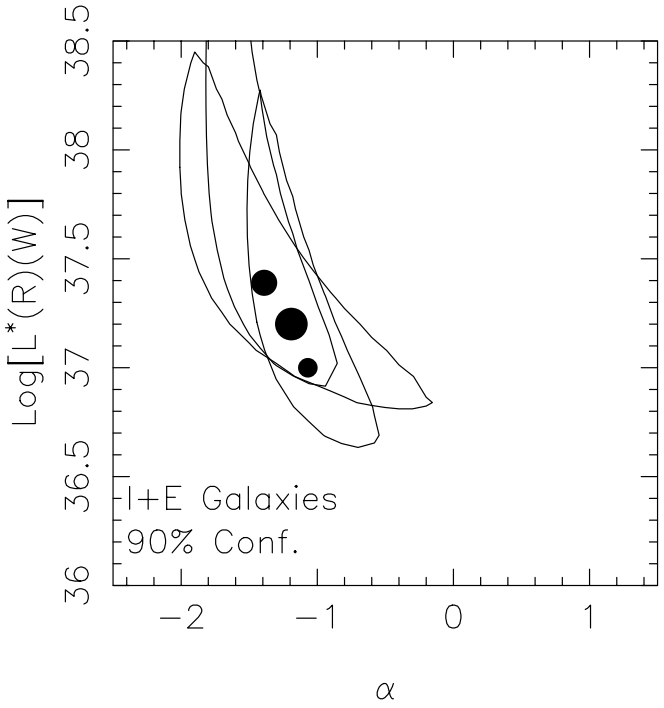

FIG. 4.—90% confidence level contours for α and $L^*(R)$ for the $\mathscr{I} + \mathscr{E}$ galaxies shown for the three redshift bins between $z = 0.25$ and 1.05. The filled circle, whose size increases with increasing redshift of the bin, denotes the maximum likelihood solution.

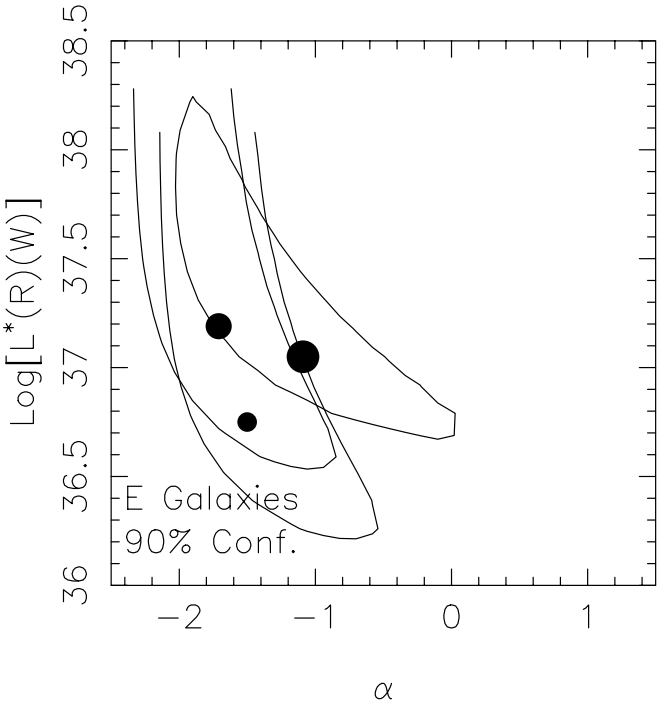

FIG. 5.—90% confidence level contours for α and $L^*(R)$ for the $\mathscr{E} + \mathscr{B}$ galaxies shown for the three redshift bins between $z = 0.25$ and 1.05. The filled circle, whose size increases with increasing redshift of the bin, denotes the maximum likelihood solution.

The results of the computation of α and $L^*(K)$ at rest-frame K are given in Tables 4 and 8. To guide our expectations, we note that, based on the mean galaxy SED parameters as a function of galaxy spectral type given in Table 3 of Cohen (2001), we might expect that $L^*(K) - L^*(R)$ will be larger for $\mathscr{A}$ galaxies than for $\mathscr{E}$ galaxies by about 0.2 dex. This is in reasonable agreement with the results of the calculations. In addition, as expected, since the absorption-line galaxies are the reddest galaxies in the sample, there the fractional contribution to the total luminosity density is slightly larger at rest-frame K than it is at R.

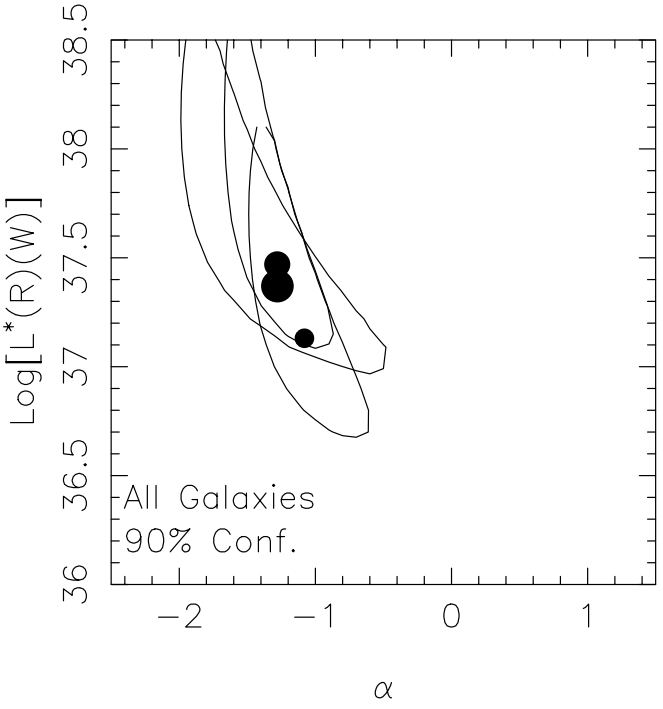

FIG. 6.—90% confidence level contours for α and $L^*(R)$ for all galaxies grouped together (except AGNs) shown for the three redshift bins between $z = 0.25$ and 1.05. The filled circle, whose size increases with increasing redshift of the bin, denotes the maximum likelihood solution.

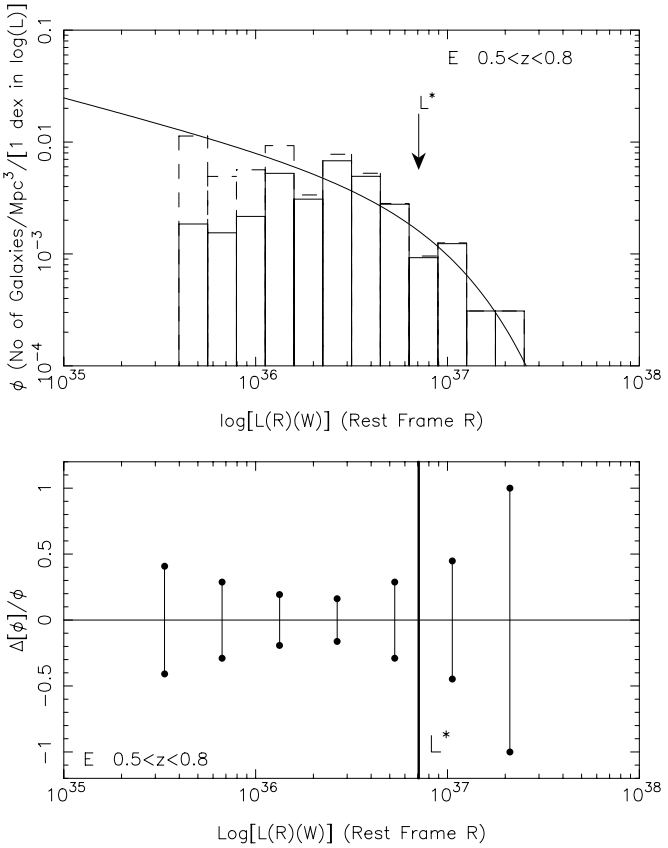

FIG. 7.—Comparison between the observed and best-fit LF for $z = 0.50$–0.80 for $\mathscr{E}$ galaxies shown in the top panel for rest-frame R. The solid lines denote the observed sample, while the dashed lines include corrections for incompleteness in the redshift survey. In the bottom panel we show $\Delta\phi/\phi$, an indication of the error arising from Poisson statistics, as a function of luminosity at rest-frame R.

LF parameters were also calculated at 2400 Å in the rest frame for galaxies with $z > 0.25$ where that regime shifts into the ground-based optical bandpass. Observed U is used to define the sample, with cutoffs of $U = 24.0$ in the Flanking Fields and 24.75 in the HDF. Here the SED model is being stretched to the extreme blue limit of its wavelength range of validity. The results of the computation of α and L^*(2400 Å) are given in Tables 9 and 10. The $\mathscr{A}$ galaxies are very faint at observed U; many have $U > 26$, well below the sample cutoff. They drop out of the sample, leaving fewer $\mathscr{A}$ galaxies in many redshift bins than the minimum adopted for an LF solution. However, these contribute very little to the total light at 2400 Å in the rest frame, and hence a negligible error is introduced into the calculation of the total luminosity density there. Only the regime $0.25 < z < 0.8$ converged well and could be used to define the mean values for α given in Table 11.

At 2400 Å, the faint-end slope, even for $\mathscr{E}$ galaxies, may be less steep than at longer wavelengths. However, the larger

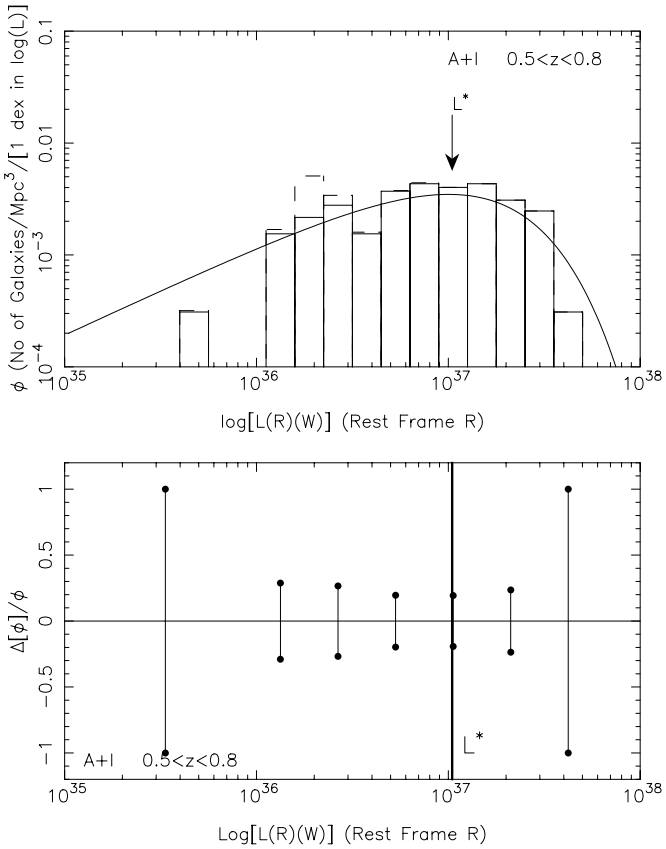

FIG. 8.—Comparison between the observed and best-fit LF for $z = 0.50$–0.80 for $\mathscr{A} + \mathscr{I}$ galaxies shown in the top panel for rest-frame R. The solid lines denote the observed sample, while the dashed lines include corrections for incompleteness in the redshift survey. In the bottom panel we show $\Delta\phi/\phi$, an indication of the error arising from Poisson statistics, as a function of luminosity at rest-frame R.

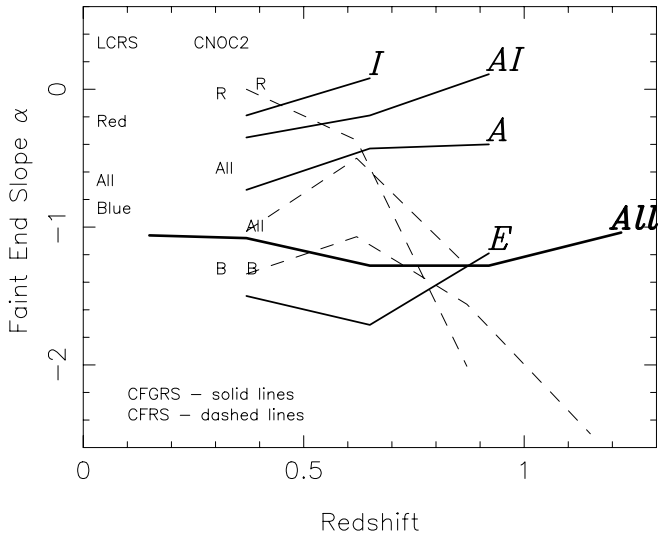

FIG. 9.—Values we have determined for α shown as a function of redshift for several galaxy spectral groupings by the thick solid curves. These are from $L^*(R)$, except for the highest redshift bin, where that of $L^*(K)$ is used. For comparison, the faint-end slopes determined by Lin et al. (1996) for the blue galaxies, the red galaxies, and the entire sample of the LCRS are shown, as are comparable values for the CNOC2 survey (Lin et al. 1999). The values of α deduced by Lilly et al. (1995) for the CFRS are indicated as the thin dashed lines.

SED errors at this rest-frame wavelength may somehow have affected the analysis to produce this apparent flattening of the LF.

5. THE BEHAVIOR OF α WITH REDSHIFT

As expected (see Figs. 1–6), the strong negative covariance between L^* and α seen in the analyses of local samples is also found here. This complicates the issue of comparing the resulting parameters among the various redshift bins and galaxy spectral groupings. Irrespective of this issue, our analysis thus far has demonstrated (see Tables 3, 4, 6, and 11) that the faint-end slope of the LFs in the redshift regime studied here shows the same general dependence on galaxy spectral type/morphological type found in numerous studies of the local LF reviewed in § 11.1. Specifically, the faint-end slope is much steeper for late-type spirals (strong emission line galaxies in the galaxy spectral classification scheme used here) than it is for galaxies without detectable emission lines.[3] This is illustrated in Figure 9, to be discussed in more detail in § 11.1.

Furthermore, α appears to be constant, to within the uncertainties due to random fluctuations given the number of galaxies in each bin, for each galaxy spectral class group over the redshift regime considered here. There is excellent agreement in the mean value of α we derive for each galaxy spectral grouping between the rest-frame U, R, and K calculations.

6. THE EVOLUTION OF L^* WITH REDSHIFT

In the next set of fits, we continue to use the standard two-parameter Schechter function model with no additional parameters. To proceed, we need to make an additional simplifying assumption. We assume, based on the results presented above, that α is in fact constant with redshift and that the variations in α within a given galaxy spectral grouping seen within Tables 3, 4, 6, and 9 are not real. An alternative approach, assuming that L^* is constant with redshift while α is allowed to vary, is explored in Appendix B.

We adopt a constant value of α for each galaxy spectral grouping independent of redshift. These values for each galaxy spectral grouping, which are from the values of α found for each redshift bin given in Tables 3, 4, 6, and 9 with $0.25 < z < 1.05$ weighted by the number of galaxies in each sample, are given in Table 11.

The specific places where this assumption is most likely not to be valid include the emission-line galaxies in the two higher redshift bins, where the galaxy spectral types becomes less distinguishable as a result of the lower quality of the spectra of such faint objects. Many galaxies in that redshift regime which might at lower redshift be considered to be of intermediate galaxy spectral type tend to get classified as $\mathscr{E}$ galaxies. The composite types $\mathscr{A} + \mathscr{I}$ and $\mathscr{I} + \mathscr{E}$ were introduced precisely to explore this issue, and indeed α for the second of these is closer to constant than it is for the $\mathscr{E}$ galaxies considered alone. In addition, the composite nature of the set consisting of all galaxies may, at higher redshift, become more dominated by the galaxies with strong emission lines, with their concomitant steeper faint-

[3] We ignore the highest redshift bin, $1.05 < z < 1.5$, where the determination of α is quite uncertain. The solution for rest-frame 2400 Å is also problematic.

TABLE 5

REST-FRAME R LF SOLUTION FOR FIXED α FOR EACH GALAXY SPECTRAL GROUPING

z Range	Total Number	Number in HDF	Number in Flanking Fields	log [$L^*(R)$] (log W)	α (fixed)	ϕ^* (Mpc^{-3})
			$\mathscr{A}$ Galaxies			
0.25–0.5	17	1	16	36.92	−0.50	0.0028 (1.63)[b]
0.5–0.8	36	6	30	37.24	−0.50	0.0033 (1.38)
0.8–1.05	19	7	12	37.37	−0.50	0.0019 (1.43)
			$\mathscr{I}$ Galaxies			
0.25–0.5	62	7	55	36.62	−0.05	0.014 (1.22)
0.5–0.8	63	8	55	36.86	−0.05	0.0066 (1.18)
0.8–1.05	14	2	12	...	...	
			$\mathscr{A} + \mathscr{I}$ Galaxies			
0.25–0.5	79	8	71	36.75	−0.20	0.017 (1.25)
0.5–0.8	99	14	85	37.02	−0.20	0.011 (1.33)
0.8–1.05	33	9	24	37.25	−0.20	0.0036 (1.33)
			$\mathscr{I} + \mathscr{E}$ Galaxies			
0.25–0.5	131	23	108	37.30	−1.25	0.0066 (1.47)
0.5–0.8	164	23	141	37.15	−1.25	0.0066 (1.54)
0.8–1.05	125	18	107	37.25	−1.25	0.0095 (1.54)
			$\mathscr{E}$ Galaxies			
0.25–0.5	69	16	53	36.71	−1.45	0.0061 (1.90)
0.5–0.8	101	15	86	36.85	−1.45	0.0052 (1.50)
0.8–1.05	111	16	95	37.32	−1.45	0.0062 (1.50)
			All Galaxies			
0.01–0.25.....	37	6	31	>36.9	−1.25	>0.0044
0.25–0.5	148	24	124	37.28	−1.25	0.0073 (1.50)
0.5–0.8	200	29	171	37.43	−1.25	0.0058 (1.54)
0.8–1.05	144	25	119	37.35	−1.25	0.0094 (1.50)
1.05–1.50.....	18	4	14	37.50[a]	−1.25	0.00054

[a] L^* could be anywhere between 37.3 and 37.7 depending on how the extrapolation for fixed α is made.

[b] These uncertainties are given in the form a factor by which ϕ^* should be multiplied or divided to obtain the 1 σ range for ϕ^*. The errors are calculated allowing both α and L^* to vary.

end slope. This would tend to produce a small decrease in α for this group with increasing z, as may be seen in Table 3, although the possible effect is not larger than the errors.

We use the contours of constant $\Delta\chi^2$ for the two-parameter solution of § 6 above (see Figs. 1–6) to reevaluate L^*, finding the value with the maximum likelihood for the appropriate fixed value of α from Table 11. This must be done for each galaxy spectral grouping at each rest-frame wavelength and for each bin in redshift. The results are given in Table 5, which is an updated version of Table 3 assuming that a fixed value of α holds for each galaxy grouping, for rest-frame R, and Tables 7, 8, and 10 for the remaining rest-frame bands analyzed here.

From the entries in Table 5 combined with the median redshift for each bin given in Table 2, we can estimate directly the change in $L^*(R)$ with redshift. Similar calculations can be carried out for each of the rest-frame colors. These piecewise values of $\Delta \log [L^*(R)]/\Delta z$ calculated over the redshift regime $0.25 < z < 1.05$ are given in Table 12, where the mean redshift of the first and last bin used defines the range Δz, as are the values for the other three rest-frame bands.

With α forced to be constant, we see an apparent increase in L^* which we believe to be valid for the $\mathscr{A}$ galaxies as well as for the $\mathscr{A} + \mathscr{I}$ composite group, as illustrated in Figure 10. The $\mathscr{E}$ galaxies also show an apparent increase in L^* with redshift, but we ascribe this to the group having an α decreasing with increasing z as the group becomes more composite, with an admixture of $\mathscr{I}$ galaxies at high redshift. Note that the biggest apparent increase in L^* for the strong emission line galaxies occurs at the highest redshift bin used. Furthermore, the apparent brightening with redshift of $\mathscr{E}$ galaxies is much less in Table 3 where α is allowed to vary with z. Also note that the solution for the composite group $\mathscr{I} + \mathscr{E}$ shows essentially no change in characteristic luminosity with redshift for a fixed α.

The characteristic luminosity of the sample as a whole is increasing slowly. In the highest redshift bin $1.05 < z < 1.5$ an uncertain extrapolation was required to determine $L^*(R)$ from the α of the maximum likelihood solution of Table 3 to the fixed α adopted; little weight can be placed on the value of α determined in this bin as the sample does not reach deep enough, and hence the results of the extrapolation must be viewed with some suspicion.

At $z \leq 0.8$, at least between rest-frame U and K, the absorption-line–dominated galaxies are the most luminous of the primary galaxy spectral groupings considered, as was already stated in C00 and Cohen (2001).

TABLE 6

SOLUTIONS FOR $L^*(U)$ AND α

z Range	Total Number	Number in HDF	Number in Flanking Fields	log [$L^*(U)$] (W)	α
			$\mathscr{A}$ Galaxies		
0.25–0.5	17	1	16	37.19 ± 0.60	-0.84 ± 0.50
0.5–0.8	36	6	30	37.15 ± 0.40	-0.66 ± 0.50
0.8–1.05	19	7	12	37.13 ± 0.30	-0.21 ± 1.30
			$\mathscr{I}$ Galaxies		
0.25–0.5	62	7	55	36.42 ± 0.25	0.30 ± 0.50
0.5–0.8	63	8	55	36.60 ± 0.20	0.24 ± 0.55
			$\mathscr{A} + \mathscr{I}$ Galaxies		
0.25–0.5	79	8	71	36.62 ± 0.20	-0.24 ± 0.35
0.5–0.8	99	14	85	36.85 ± 0.15	-0.30 ± 0.40
0.8–1.05	33	9	24	37.02 ± 0.35	0.00 ± 0.80
			$\mathscr{I} + \mathscr{E}$ Galaxies		
0.25–0.5	131	23	108	36.74 ± 0.25	-1.03 ± 0.20
0.5–0.8	164	23	141	36.99 ± 0.30	-1.27 ± 0.25
0.8–1.05	125	18	107	36.85 ± 0.25	-0.85 ± 0.45
			$\mathscr{E}$ Galaxies		
0.25–0.5	69	16	53	36.70 ± 0.45	-1.51 ± 0.25
0.5–0.8	101	15	86	37.03 ± 0.65	-1.71 ± 0.20
0.8–1.05	111	16	95	36.76 ± 0.25	-0.85 ± 0.55
			All Galaxies		
0.01–0.25.....	37	6	31	$>36.58 \pm 0.40$[a]	-0.90 ± 0.20
0.25–0.5	148	24	124	36.90 ± 0.20	-1.09 ± 0.15
0.5–0.8	200	29	171	37.17 ± 0.20	-1.22 ± 0.20
0.8–1.05	144	25	119	37.07 ± 0.40	-1.12 ± 0.35
1.05–1.50.....	18[b]	4	14	37.41 ± 0.50	-0.73 ± 1.20

[a] Assigned as a lower limit as a result of selection criteria for HDF.
[b] Galaxies in the HDF with $23.5 < R < 24$ were eliminated.

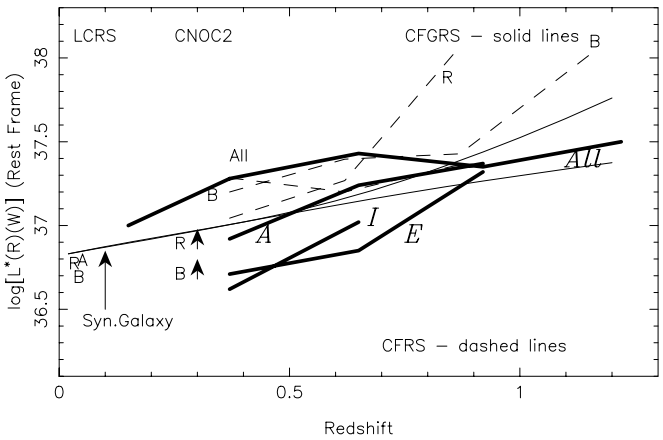

FIG. 10.—Thick solid curves show $L^*(R)$ (W) as a function of redshift derived here (see Table 5) for the $\mathscr{A}$ and $\mathscr{E}$ galaxy spectral groupings, as well as for our entire sample. The values of $L^*(R)$ for the complete sample, as well as that subdivided into "blue" and "red" (equivalently, "emission" and "no emission") galaxies, from the LCRS (Lin et al. 1996), CNOC2 (Lin et al. 1999), and CFRS (Lilly et al. 1995) are shown for comparison. The CFRS values are indicated by the dashed lines. The thin solid lines denote the predicted evolution of an elliptical and an Sc galaxy from the models of Poggianti (1997) as a function of redshift.

6.1. *Formal Solution for the Evolution of L* with Redshift*

We attempt to derive in a more formal way the evolution of L^* to verify the results of the previous section using a global fit. We introduce the parameter Q used by Lin et al. (1999), among others, where $L^*(z) = L^*(z = 0) \times 10^{Qz}$. Given the modest size of our sample and the large redshift range, issues of the stability of any solution suggest that we need to simplify things somewhat and avoid doing a full three-parameter (L^*, α, Q) fit for each rest wavelength considered here. To accomplish this, taking rest-frame R as an example, first we fix α to the mean value given above for each galaxy spectral grouping in Table 11. Second, we fix the value of $L^*(R)$ at the mean redshift of the bin $0.5 < z < 0.8$ to the value obtained for that redshift bin in Table 5. This redshift bin was chosen because it is more populated than the lower z bins. We are then left with only a single unknown, the parameter Q. We solve for the most likely value of Q.

In this solution, we have assumed a simple parametric form for the evolution of L^* with redshift and also assumed a value for L^* at some particular redshift, as well as continued our assumption of a fixed value for α. This is the price for avoiding the use of individual redshift bins, each with

TABLE 7

REST-FRAME U LF SOLUTION FOR FIXED α FOR EACH GALAXY SPECTRAL GROUPING

z Range	Total Number	Number in HDF	Number in Flanking Fields	log [$L^*(U)$] (log W)	α (fixed)	ϕ^* (Mpc^{-3})
			$\mathscr{A}$ Galaxies			
0.25–0.5	17	1	16	36.89	−0.60	0.241E−2
0.5–0.8	36	6	30	37.10	−0.60	0.282E−2
0.8–1.05	19	7	12	37.30	−0.60	0.164E−2
			$\mathscr{I}$ Galaxies			
0.25–0.5	62	7	55	36.42	0.30	0.144E−1
0.5–0.8	63	8	55	36.56	0.30	0.655E−2
			$\mathscr{A} + \mathscr{I}$ Galaxies			
0.25–0.5	79	8	71	36.62	−0.25	0.159E−1
0.5–0.8	99	14	85	36.82	−0.25	0.978E−2
0.8–1.05	33	9	24	37.11	−0.25	0.340E−2
			$\mathscr{I} + \mathscr{E}$ Galaxies			
0.25–0.5	131	23	108	36.78	−1.05	0.126E−1
0.5–0.8	164	23	141	36.78	−1.05	0.107E−1
0.8–1.05	125	18	107	36.92	−1.05	0.130E−1
			$\mathscr{E}$ Galaxies			
0.25–0.5	69	16	53	36.45	−1.30	0.744E−2
0.5–0.8	101	15	86	36.60	−1.30	0.729E−2
0.8–1.05	111	16	95	37.00	−1.30	0.863E−2
			All Galaxies			
0.01–0.25.....	37	6	31	>37.15	−1.15	>0.568E−2
0.25–0.5	148	24	124	37.03	−1.15	0.929E−2
0.5–0.8	200	29	171	37.05	−1.15	0.834E−2
0.8–1.05	144	25	119	37.05	−1.15	0.118E−1
1.05–1.50.....	18	4	14	37.65[a]	−1.15	0.445E−3[a]

[a] Extremely uncertain values.

their small samples and large uncertainties, used in the previous section (§ 6) to derive the evolution of L^* in a piecewise fashion. If we were sure we could match our photometry and galaxy spectral groups onto those of local samples, the much larger local samples could be used to provide the benchmark luminosity $L^*(z = 0)$. However, this is not the case, and we must use one of our own redshift bins as the benchmark.

The results of this exercise are given in Table 13. The evolutionary rates over the interval $0.25 < z < 1.05$ given in this table are very similar for rest-frame U, R, and K. They confirm the simpler analysis given in the previous section. Strong evolution in $L^*(R)$ is found for the same specific galaxy spectral groupings, $\mathscr{A}$, $\mathscr{I}$, $\mathscr{A} + \mathscr{I}$, and $\mathscr{E}$, where Q ranges from 0.6 to 1.2 as in § 6. As described above, the apparent high Q found for the $\mathscr{E}$ galaxies is believed to be spurious. Little/no evolution in the characteristic luminosity of the same set of two galaxy spectral groupings ($\mathscr{I} + \mathscr{E}$ and "All") as were approximately constant in the qualitative test of the previous section is seen in this more quantitative test. Similar results are obtained if $L^*(R)$ is held fixed to the value found for the lowest redshift bin at that mean redshift.

The 1 σ single-parameter errors are given in the last column of Table 13. They suggest that while the overall trends of the evolution of $L^*(R)$ with redshift can be discerned through analysis of our limited data set, a much larger sample of galaxies will be needed to determine this to an accuracy of 10%.

To verify the above results, we have carried out a solution allowing all three parameters, L^*, α, and Q, to vary for each of the three rest-frame bands U, R, and K. We do this only for the most populous galaxy spectral groupings, $\mathscr{I} + \mathscr{E}$ and "All," and obtain the results labeled "(3p)" in Table 13, which are in agreement to within the uncertainties with the values given in the same table for the somewhat more constrained solution procedure described above. The values from the three-parameter solution are to be preferred and are those used subsequently. The errors among these three quantities show strong negative covariances, particularly between L^* and Q.

With the improvement of a three-parameter fit, we are still forcing α to be a constant independent of redshift. As a result of the small size of our sample, even in the best case, our 1 σ uncertainty in α is ± 0.15. Testing rest-frame R as an example, we find that adoption of a value for α that is 0.15 too large will result in an underestimate of $L^*(R)$ by 0.35 dex for $\mathscr{E}$ galaxies but only by 0.05 dex for $\mathscr{A}$ galaxies. This striking difference arises because of the differing shapes of the error contours. Very steep faint-end slopes are often accompanied by error contours which are much closer to vertical in the α-L^* plane, as is apparent from comparing Figure 2 with Figure 5. Thus, a small trend in α with z which can be hidden within our uncertainties may still be enough

TABLE 8

REST-FRAME K LF SOLUTION FOR FIXED α FOR EACH GALAXY SPECTRAL GROUPING

z Range	Total Number	Number in HDF	Number in Flanking Fields	log [$L^*(K)$] (log W)	α (fixed)	ϕ^* (Mpc^{-3})
			$\mathscr{A}$ Galaxies			
0.25–0.5	15	0	15	36.50	−0.10	0.374E−2
0.5–0.8	36	6	30	37.00	−0.10	0.336E−2
0.8–1.05	19	7	12	37.15	−0.10	0.164E−2
			$\mathscr{I}$ Galaxies			
0.25–0.5	60	7	53	36.45	−0.20	0.138E−1
0.5–0.8	62	5	55	36.70	−0.20	0.623E−2
0.8–1.05	16	2	14	37.10	−0.20	0.130E−2
			$\mathscr{A}$ + $\mathscr{I}$ Galaxies			
0.25–0.5	75	7	68	36.50	−0.30	0.164E−1
0.5–0.8	98	13	85	36.90	−0.30	0.875E−2
0.8–1.05	35	9	26	37.25	−0.30	0.256E−2
			$\mathscr{I}$ + $\mathscr{E}$ Galaxies			
0.25–0.5	115	22	93	36.95	−1.20	0.698E−2
0.5–0.8	147	17	130	36.95	−1.20	0.540E−2
0.8–1.05	121	15	106	37.20	−1.20	0.435E−2
			$\mathscr{E}$ Galaxies			
0.25–0.5	55	15	40	36.30	−1.35	0.640E−2
0.5–0.8	85	10	75	36.50	−1.35	0.496E−2
0.8–1.05	105	13	92	37.20	−1.35	0.299E−2
			All Galaxies			
0.01–0.25.....	30	5	25	>37.0	−1.15	>0.414E−2
0.25–0.5	130	22	108	37.00	−1.15	0.840E−2
0.5–0.8	183	23	160	37.20	−1.15	0.559E−2
0.8–1.05	140	22	118	37.30	−1.15	0.481E−2
1.05–1.50.....	27	10	17	37.40	−1.15	0.378E−3

to produce errors in L^* of 0.2 dex for galaxy spectral groupings with very steep faint-end slopes, while L^* determinations for galaxy spectral groupings with flatter faint-end slopes should be more accurate and less dependent on the exact choice of α.

6.2. *Overall Summary for the Behavior of L**

The galaxy spectral groups $\mathscr{A}$, $\mathscr{I}$, $\mathscr{A}$ + $\mathscr{I}$, and $\mathscr{E}$ all show substantial brightening with redshift over the range from 0.24 to 2.2 μm. The composite group $\mathscr{I}$ + $\mathscr{E}$ and the group consisting of all galaxies show a slower increase in luminosity with redshift except at 2400 Å. The rise in L^* found here for the galaxy spectral groupings with flatter faint-end slopes is believed to be real. However, we suggest that the large apparent brightening seen for the $\mathscr{E}$ spectral group is spurious and is due to mixing of $\mathscr{I}$ with $\mathscr{E}$ galaxies in the higher redshift bins where these two galaxy classes become essentially indistinguishable. This mixing would produce almost undetectable changes in the composite value of α, given our uncertainties.

We thus view the subdivision of the sample into galaxy spectral groupings whose results are most likely to be valid as the $\mathscr{A}$ with the $\mathscr{I}$ + $\mathscr{E}$ groups. Those, as well as the group containing all the galaxies, will be the groups emphasized in the remainder of this work.

7. THE EVOLUTION OF NUMBER DENSITY WITH REDSHIFT

The final step in this analysis is to compute the normalization constant for the LF. The calculations are carried out with α fixed at the mean value adopted for each galaxy spectral grouping (given in Table 11) and the resulting luminosities from Table 5. For rest-frame R only, we give 1 σ errors as a multiplier to be applied to ϕ^*. These were calculated utilizing the 1 σ error contours of the two-parameter LF solutions. We take the L^* and α from these contours at the ends of the major and minor axes of the error contour. We then propagate these values through the codes to calculate four values of ϕ^*. We take the average of the absolute values of the fractional deviations with respect to the nominal value as the 1 σ error. This is an approximation for the true σ but should be close enough for our purposes, given our small sample size.

It is important to stress that the errors given in Table 5 include variations in L^* and α, as well as the term arising from Poisson statistics. Although the numbers of galaxies in some of the bins are quite small, the contribution to the total error of this last term is generally small. These errors have *not* been calculated assuming fixed values of α but represent the full range of likelihood with both parameters allowed to vary.

TABLE 9

SOLUTIONS FOR L^*(2400 Å) AND α

z Range	Total Number	Number in HDF	Number in Flanking Fields	log [L^*(2400Å)] (W)	α
			$\mathscr{A}$ Galaxies		
0.25–0.5	8	1	7	...	...
0.5–0.8	15	3	13	36.40 ± 0.40[a]	-1.00 ± 0.70[a]
0.8–1.05	5	1	4	...	...
			$\mathscr{I}$ Galaxies		
0.25–0.5	56	8	48	36.12 ± 0.25	-0.28 ± 0.45
0.5–0.8	51	8	44	36.65 ± 0.30	-0.87 ± 0.35
0.8–1.05	10	1	9	...	...
			$\mathscr{A} + \mathscr{I}$ Galaxies		
0.25–0.5	64	9	55	36.10 ± 0.20	-0.27 ± 0.35
0.5–0.8	66	11	57	36.62 ± 0.35	-0.93 ± 0.40
0.8–1.05	15	2	13	36.19 ± 0.30	1.94 ± 1.20
			$\mathscr{I} + \mathscr{E}$ Galaxies		
0.25–0.5	121	25	96	36.05 ± 0.15	-0.33 ± 0.30
0.5–0.8	140	23	120	36.51 ± 0.20	-0.76 ± 0.30
0.8–1.05	110	18	95	36.25 ± 0.20	1.08 ± 0.65
			$\mathscr{E}$ Galaxies		
0.25–0.5	65	17	48	36.00 ± 0.25	-0.44 ± 0.40
0.5–0.8	89	15	76	36.42 ± 0.20	-0.70 ± 0.35
0.8–1.05	100	15	76	36.25 ± 0.10	1.14 ± 0.60
			All Galaxies		
0.01–0.25.....	[b]	[b]	...	...	...
0.25–0.5	129	26	103	35.86 ± 0.15	-0.43 ± 0.25
0.5–0.8	155	26	133	36.49 ± 0.15	-0.77 ± 0.20
0.8–1.05	115	19	99	36.25 ± 0.10	1.14 ± 0.70
1.05–1.50.....	22	12	12	36.55 ± 0.35	-0.17 ± 1.00

[a] These are 1 σ one-parameter errors throughout. See Figs. 1–6 for the two-parameter error contours.
[b] Not observable from the ground at $0.01 < z < 0.25$.

To understand the behavior of the uncertainty for ϕ^* shown in Table 5, consider an idealized sample of galaxies which is complete and which reaches as faint as L(min), where $L(\text{min}) \sim 0.1L^*$. The error in ϕ^* will depend on α. For α large and positive, the LF approaches a δ-function. As long as the δ-function is located at $L^* > L$(min), the error in ϕ^* will be zero. However, for the steep faint-end slopes found for the LFs of $\mathscr{E}$ galaxies, the integral of the LF will change significantly for a small change in α, and hence the uncertainty in ϕ^* will be large. For a very deep sample where $L(\text{min}) \lesssim 0.01L^*$, a situation not achieved in the present sample, the changes in the integral are small as α is varied even for steep faint-end slopes. For a fixed α and L(min), as L^* increases, ϕ^* decreases, and again the change in the integral is larger for LFs with steeper faint-end slopes.

Similar calculations were carried out to evaluate ϕ^* at each of the other rest-frame wavelengths considered here; the results are reported in the last column of Tables 7, 8, and 10.

As an approximation to gain insight, we assume that at any rest-frame wavelength and for a particular galaxy spectral grouping, galaxy LFs change with redshift only through variations of L^*. With this assumption, $N = \phi^* f(\alpha)$. We can then directly compare the number densities as a function of redshift within the entries for a particular galaxy spectral grouping (i.e., a particular choice of α) simply by comparing the derived values of ϕ^*.

We find that the comoving number density of $\mathscr{A}$ galaxies is constant between $z = 0.4$ and 0.6 but then declines by 40% at a mean $z = 0.9$. We have calculated using our SED formalism the redshift at which a normal $\mathscr{A}$ galaxy with a typical SED from Cohen (2001) becomes fainter than the cutoff in the Flanking Field for an L^* galaxy. At observed R this is $z \sim 0.9$, and at observed K this is $z \sim 1.25$. Thus, it is only to be expected that almost all of the absorption-line galaxies will be fainter than the faint-end cutoff adopted at observed R for $z > 0.9$, and this produces a drastic drop in the number of $\mathscr{A}$ galaxies in the sample. We emphasize that this happens for the nominal SED of an absorption-line galaxy.

One way of checking that the comoving number density of $\mathscr{A}$ galaxies is actually constant, at least out to $z = 1.05$, is to calculate the luminosity density from such galaxies in each redshift bin, but including only such galaxies more luminous than $L_{\text{min}}(R)$. Comparison of luminosity densities is much more robust than comparison of individual LF parameters such as α or L^*. We do this by directly summing the $L(R)$ for the $\mathscr{A}$ observed galaxies in the sample (no

TABLE 10

REST-FRAME 2400 Å LF SOLUTION FOR FIXED α FOR EACH GALAXY SPECTRAL GROUPING

z Range	Total Number	Number in HDF	Number in Flanking Fields	log [L^*(2400 Å)] (log W)	α (fixed)	ϕ^* (Mpc^{-3})
			$\mathscr{I}$ Galaxies			
0.25–0.5	56	8	48	36.28	−0.55	0.118E−1
0.5–0.8	51	8	44	36.44	−0.55	0.624E−2
0.8–1.05	12	1	12	...	...	...
			$\mathscr{A}$ + $\mathscr{I}$ Galaxies			
0.25–0.5	64	9	55	36.29	−0.60	0.126E−1
0.5–0.8	66	11	57	36.40	−0.60	0.842E−2
0.8–1.05	15	2	14	36.85	−0.60	0.124E−2
			$\mathscr{I}$ + $\mathscr{E}$ Galaxies			
0.25–0.5	121	25	96	36.17	−0.55	0.291E−1
0.5–0.8	140	23	120	36.39	−0.55	0.191E−1
0.8–1.05	105	18	89	36.60	−0.55	0.178E−1
			$\mathscr{E}$ Galaxies			
0.25–0.5	65	17	48	36.10	−0.60	0.166E−1
0.5–0.8	89	15	76	36.36	−0.60	0.126E−1
0.8–1.05	100	17	85	36.60	−0.60	0.165E−1
			All Galaxies			
0.25–0.5	129	26	103	36.18	−0.60	0.292E−1
0.5–0.8	155	26	133	36.37	−0.60	0.211E−1
0.8–1.05	115	19	99	36.60	−0.60	0.180E−1
1.05–1.50.....	22	12	12	36.65	−0.60	0.360E−2

TABLE 11

MEAN α ADOPTED FOR EACH GALAXY SPECTRAL GROUPING

		Mean α			
Spectral Group	Typical N(Gal) (z = 0.25–1.05)	Rest-Frame U (z = 0.25–1.05)	Rest-Frame R (z = 0.25–1.05)	Rest-Frame K (z = 0.25–1.05)	Rest-Frame 2400 Å (z = 0.25–0.8)
$\mathscr{A}$	70	−0.60 ± 0.45	−0.50 ± 0.40	−0.10 ± 0.30	...
$\mathscr{I}$	140	0.30 ± 0.35	−0.05 ± 0.35	−0.20 ± 0.25	(−0.55 ± 0.30)
$\mathscr{A}$ + $\mathscr{I}$	210	−0.25 ± 0.25	−0.20 ± 0.30	−0.30 ± 0.20	(−0.60 ± 0.25)
$\mathscr{I}$ + $\mathscr{E}$	385	−1.05 ± 0.20	−1.25 ± 0.15	−1.20 ± 0.15	(−0.60 ± 0.20)
$\mathscr{E}$	245	−1.30 ± 0.25	−1.45 ± 0.25	−1.35 ± 0.20	(−0.60 ± 0.25)
All	495	−1.15 ± 0.15	−1.25 ± 0.15	−1.15 ± 0.10	(−0.60 ± 0.15)

TABLE 12

PIECEWISE CALCULATION OF LF EVOLUTION FROM z = 0 TO 1

Galaxy Types	Δ{log [$L^*(U)$]}[a] (dex)	Δ{log [$L^*(R)$]}[a] (dex)	Δ{log [$L^*(K)$]}[a] (dex)	Δ{log [L^*(2400 Å)]}[b] (dex)
$\mathscr{A}$	0.8	0.9	1.3	...
$\mathscr{I}$[c]	0.3	1.0	1.3	...
$\mathscr{A}$ + $\mathscr{I}$	1.1	1.0	1.5	0.4
$\mathscr{I}$ + $\mathscr{E}$	0.3	0.0	0.5	0.7
$\mathscr{E}$	1.1	1.2[d]	1.8[d]	0.9
All	0.0	0.2	0.6	0.6

[a] The regime $0.25 < z < 1.05$ is used for this calculation.
[b] Only the regime $0.25 < z < 0.80$ is used for this calculation.
[c] Quite uncertain as a result of a low number of $\mathscr{I}$ galaxies in the $0.8 < z < 1.05$ bin.
[d] The values listed for this entry are believed to be spurious. See the text for details.

TABLE 13

SOLUTION FOR Q, THE LF EVOLUTION FROM $z = 0$ TO 1[a]

Galaxy Types	Number of Galaxies	Number in HDF	Number in Flanking Fields	log [$L^*(W)$] (at $z = 0.60$)	α (fixed)	Q
			Rest-Frame U			
$\mathscr{A}$	72	14	58	37.10	−0.60	0.55 ± 0.70[b]
$\mathscr{I}$[c]	139	17	122	36.56	0.30	1.45 ± 0.45
$\mathscr{A} + \mathscr{I}$	211	31	180	36.82	−0.25	1.20 ± 0.45
$\mathscr{I} + \mathscr{E}$	420	64	356	36.78	−1.05	0.20 ± 0.40
$\mathscr{I} + \mathscr{E}$(3p)	420	64	356	36.68 ± 0.30	-1.15 ± 0.15	0.46 ± 0.30
$\mathscr{E}$	281	47	234	36.60	−1.30	0.85 ± 0.40
All	492	78	414	37.05	−1.15	-0.15 ± 0.40
All (3p)	492	78	414	36.88 ± 0.25	-1.20 ± 0.15	0.30 ± 0.25
			Rest-Frame R			
$\mathscr{A}$	72	14	58	37.24	−0.50	0.62 ± 0.70
$\mathscr{I}$[c]	139	17	122	36.86	−0.05	1.25 ± 0.50
$\mathscr{A} + \mathscr{I}$	211	31	180	37.02	−0.20	1.18 ± 0.45
$\mathscr{I} + \mathscr{E}$	420	64	356	37.15	−1.25	-0.02 ± 0.40
$\mathscr{I} + \mathscr{E}$ (3p)	420	64	356	37.16 ± 0.35	-1.30 ± 0.15	0.21 ± 0.35
$\mathscr{E}$	281	47	234	36.85	−1.45	0.90 ± 0.40
All	492	78	414	37.43	−1.25	-0.24 ± 0.40
All (3p)	492	78	414	37.24 ± 0.25	-1.30 ± 0.10	0.06 ± 0.35
			Rest-Frame K			
$\mathscr{A}$	71	14	57	37.00	−0.10	0.69 ± 0.70
$\mathscr{I}$[c]	138	16	122	36.70	−0.20	1.45 ± 0.50
$\mathscr{A} + \mathscr{I}$	209	30	179	36.90	−0.30	1.39 ± 0.50
$\mathscr{I} + \mathscr{E}$	387	58	329	36.95	−1.20	0.27 ± 0.50
$\mathscr{I} + \mathscr{E}$ (3p)	387	58	329	36.90 ± 0.40	-1.30 ± 0.20	0.50 ± 0.50
$\mathscr{E}$	249	42	207	36.50	−1.35	1.32 ± 0.50
All	458	62	386	37.20	−1.15	-0.01 ± 0.50
All (3p)	458	62	386	37.05 ± 0.40	-1.25 ± 0.20	0.42 ± 0.50
			Rest-Frame 2400 Å			
$\mathscr{I} + \mathscr{E}$	371	66	311	36.37	−0.55	1.17 ± 0.30
$\mathscr{E}$	254	49	209	36.36	−0.60	1.31 ± 0.30
All	399	71	335	36.37	−0.60	1.24 ± 0.25

[a] The solution for Q utilizes the regime $0.25 < z < 1.05$.
[b] These are single-parameter 1 σ errors.
[c] Quite uncertain as a result of a low number of $\mathscr{I}$ galaxies in the $0.8 < z < 1.05$ bin.

weighting is applied), adopting $L_{\rm min} = 36.0 + 0.6z$. This yields values of 0.57, 1.16, and 0.86×10^{36} W Mpc^{-3} for the redshift bins 0.25–0.5, 0.5–0.8, and 0.8–1.05, respectively. The selection criteria adopted for the HDF itself ("no bright galaxies") probably produce the low value in the lowest redshift bin. The values for the two higher redshift bins agree to within 25%. Since luminous $\mathscr{A}$ galaxies are highly clustered, clustering could easily account for this difference.

Daddi, Cimitti, & Renzini (2000) have evaluated the surface density of extremely red objects (EROs) with colors corresponding to passively evolving elliptical galaxies in the latest large-area deep infrared imaging surveys (both their own and those of Thompson et al. 1999) and conclude that there is good agreement in all respects between the properties of the EROs and those predicted for ellipticals at $z > 1$.

The comoving density of galaxies with emission lines does not change by more than 20% out to $z = 1.05$ based on the $\mathscr{I} + \mathscr{E}$ and $\mathscr{E}$ galaxy spectral groupings. The comoving number density of the entire sample of galaxies is dominated by the $\mathscr{E}$ galaxies. The lowest redshift bin ($z < 0.25$) is low by a factor of ~ 2, which is not surprising considering the deliberate choice of the HDF as a region devoid of bright (i.e., nearby) galaxies. Ignoring that bin, the volume density is constant to within the uncertainties until the highest redshift bin, $1.05 < z < 1.5$, at which point it falls drastically, by a factor of ~ 10. This is in agreement with Figure 6 of C00, a plot of observed R magnitude versus z for the galaxies in this sample, which gives the strong visual impression that there is a deficit of galaxies at $z > 1$.

The situation at the highest redshift bin is difficult to evaluate. There is a litany of problems here, ranging from not seeing very deep in the LF to having to extrapolate rest-frame R when it corresponds to an observed wavelength of 2600 Å, thus requiring trust in the SED model perhaps beyond that warranted. It must also be recalled that the grouping of all galaxies is a sum of galaxies of several different spectral groups whose relative contributions change as a function of redshift. It is thus the most likely galaxy spectral grouping of those we use here to

violate the assumptions made here about how galaxy LFs evolve with redshift, specifically that α remains constant and that LFs change only through variation of L^*.

7.1. *The Impact of the High-z Weights*

We can estimate the number of objects that are missing redshifts in the R-selected sample. Overall our redshift survey is $\sim 93\%$ complete to the stated limits ($R = 24$ in the HDF, $R = 23.5$ in the Flanking Fields). There are about 735 objects with redshifts in the region of the HDF, including Galactic stars, but we need the number that fall within these photometric limits. If we ignore the very small number of higher z objects within these photometric limits, we deduce that there are about 50 objects missing from the redshift survey. In this weighting scheme, those objects are all put into the highest redshift ($1.05 < z < 1.5$) bin, rather than into any of the lower z bins.

For each additional rest-frame bandpass in which we calculate the LF, the effective number of missing galaxies is derived by examining the total number of objects used and the total weight W under the magnitude weight scheme. We calculate the part of W due to objects which are within the photometric limits of the survey but which do not have spectroscopic redshifts (the "missing" galaxies). This calculation carried out at rest-frame K suggests that the number of galaxies in the highest redshift bin, which is 27 in this case, must be increased by ~ 100.

The highest redshift bin is very sparsely populated. As a result of the completeness limits adopted, the R-selected sample in this redshift bin contains only 24 objects of the 38 galaxies with $1.05 < z < 1.5$ in the redshift catalog. (The K-selected sample contains 27 galaxies in this z bin.) Six of these 24 galaxies are in the HDF with $23.5 < z < 24$ and hence have $W \sim 9.5$. These were excluded from the rest-frame R analysis but not from the rest-frame K analysis.

Thus, the impact of adopting the high-z weighting scheme is dramatic in the highest redshift bin, increasing the number of objects by factors of ~ 4. This will provide the maximum possible correction factor to ϕ^* for the highest redshift bin. Since the redshift survey is very complete, the impact on the lower z bins of adopting this weighting scheme is small. Less than 15% of the total weight in the redshift bins up to $z = 1.05$ in the R-selected sample comes from objects that are not observed. The number of objects in all lower redshift bins should be decreased at the same time by $\sim 20\%$ for the $0.8 < z < 1.05$ bin and by 8% for the $0.25 < z < 0.5$ redshift bin for the R-selected sample, with slightly higher values prevailing for the K selected sample.

7.2. *Correction Factors for the Number Density in the Highest Redshift Bin*

At first glance, as shown in § 7.1, the redshift regime $1.05 < z < 1.5$ has a comoving number density of galaxies drastically smaller (by a factor of 10 or more) than that of the lower redshift bins. Our approach is to make our best-effort estimate of the correction factors that can be applied, leaning toward trying to achieve a maximum comoving number density, and to see if these correction factors can realistically be made large enough to achieve constant comoving number density. The biggest correction factor will come from adopting the high-z weighting scheme discussed above for the galaxies missing spectroscopic redshifts but within the adopted limits for the photometric survey. We adopt the values given in the previous section, i.e., the R sample then has ~ 100 galaxies in the highest redshift bin, the K sample ~ 125 galaxies. Note that this is a firm upper limit to the correction.

We can easily be missing another 10% of the galaxies through problems in the photometry at these faint levels, overlapping images which have not been properly resolved, etc. Note that this is 10% of *all* galaxies in the sample, or perhaps more appropriately 10% of all faint galaxies in the sample, *not* 10% of the galaxies in the highest redshift bin. Just as for the galaxies missing redshifts, we apply this correction assuming that all these galaxies (55 galaxies) are at high redshift and to be added to the highest redshift bin only. This factor could be underestimated slightly, so since we are going for the maximum believable correction, we apply a 15% correction, which is equivalent to adding 80 galaxies, to the highest redshift bin. (It is here that a sample defined exclusively through *HST* imaging, with much better characteristic spatial resolution, would be superior. We have repeatedly requested *HST* imaging of the HDF Flanking Fields.)

We must then add in all the $\mathscr{A}$ galaxies which are mostly, at this high redshift, fainter than the photometric cutoffs adopted. Absorption-line galaxies constitute roughly one-sixth of the total R-selected sample in the lower redshift bins, and we assume that this should apply in the highest redshift bin as well. This makes the membership of the highest redshift bin be ~ 200 galaxies and brings the comoving number density in the bin $1.05 < z < 1.5$ to within 30% of the number density for lower redshifts. We regard this as close enough, given the errors.

Furthermore, at $z = 1.5$, R in the observed frame corresponds to a wavelength of 2600 Å, which is at the limit of validity at the blue end of our SEDs. (See Cohen 2001 for a more detailed discussion of the limitations of our SED model.) The errors for L(2400 Å) are larger than those of other bands considered here because of the uncertainty of the SED model there.

This combination of factors does just barely succeed in raising the population of the highest redshift bin $1.05 < z < 1.5$ to the point where it is consistent with constant number density of galaxies throughout the sample volume. We emphasize that we have pushed each factor to its maximum to accomplish this. We have perhaps pressed these factors beyond the tolerance of the referee, to which the author can only reply that after looking at the images and the spectra and checking object by object over the course of the past few years, she believes that such large correction factors cannot be ruled out. It is not possible for the comoving galaxy number density at luminosities near L^* to have been significantly higher at $z \sim 1.3$ than it is at present.

To summarize the conclusion of this discussion, assuming that no large error has been introduced by fixing α for the highest redshift bin, the apparent deficit of luminous galaxies with $z > 1$ in our earlier papers is probably *not* real, but this requires stretching the correction factors for various sample selection issues to their maximum credible values. This result needs to be verified with a deeper and much larger redshift sample accompanied by a photometric catalog based on better spatial resolution images than those available to us.

TABLE 14

PREDICTED VERSUS ACTUAL GALAXY COUNTS

GALAXY TYPES	$0.01 < z < 0.25$		$0.25 < z < 0.5$		$0.5 < z < 0.8$		$0.8 < z < 1.05$		$1.05 < z < 1.5$	
	Observed	Predicted	Observed	Predicted	Observed	Predicted	Observed	Predicted	Observed	Predicted
Rest-Frame U[a]										
$\mathscr{A}$	...	...	17	18	36	46	19	24	...	...
$\mathscr{I}$	...	...	62	64	63	66	...	...	...	...
$\mathscr{A} + \mathscr{I}$	...	...	79	80	99	112	33	39	...	...
$\mathscr{I} + \mathscr{E}$	...	...	131	146	164	205	125	162	...	...
$\mathscr{E}$	...	...	69	78	101	131	111	143	...	...
All	37	45	148	145	200	250	144	193	18[b]	29
Rest-Frame R[a]										
$\mathscr{A}$	...	...	17	18	36	42	19	17	...	...
$\mathscr{I}$	...	...	62	59	63	62	...	...	...	...
$\mathscr{A} + \mathscr{I}$	...	...	79	83	99	118	33	32	...	...
$\mathscr{I} + \mathscr{E}$	...	...	131	142	164	187	125	152	...	...
$\mathscr{E}$	...	...	69	86	101	120	111	149	...	...
All	37	32	148	151	200	223	144	161	18[b]	14
Rest-Frame K[c]										
$\mathscr{A}$	...	...	15	17	36	37	19	19	...	...
$\mathscr{I}$	...	...	60	67	62	69	16	16	...	...
$\mathscr{A} + \mathscr{I}$	...	...	75	84	98	107	35	35	...	...
$\mathscr{I} + \mathscr{E}$	...	...	115	152	147	204	121	157	...	...
$\mathscr{E}$	...	...	55	86	85	131	105	155	...	...
All	30	32	130	168	183	239	183	185	27	30
Rest-Frame 2400 Å[c]										
$\mathscr{I}$	...	...	56	59	51	57	...	...	...	...
$\mathscr{I} + \mathscr{E}$	...	...	129	135	140	171	105	129	...	...
$\mathscr{E}$	...	...	65	71	89	111	100	127	...	...
All	...	...	129	138	155	184	115	123	22	28

[a] The observed number of galaxies at rest-frame R is calculated to an observed magnitude of $R = 23.5$.
[b] Six galaxies in the HDF with $23.5 < R < 24$ have been eliminated. See text for details.
[c] The observed number of galaxies at rest-frame K is calculated to an observed magnitude of $K = 20.75$.
[d] The observed number of galaxies at rest-frame 2400 Å is calculated to an observed magnitude of $U = 24.0$.

7.3. *Comparison of Observed and Predicted Properties of the Sample*

As a check on the validity of our LF modeling, we utilize the parameters determined above, together with the volume of the cone of our survey through each of the redshift bins, to predict the number of galaxies that should have been observed in our sample in the various galaxy spectral groupings in each of the redshift bins. In these calculations, we adopt a magnitude cutoff of $R = 23.5$ (R in the observed frame) and find the corresponding value of $L(U)$ and $L(R)$ using the mean SED parameters for each galaxy spectral type given in Cohen (2001). Similar calculations are done for the rest-frame K sample selected at observed K with a cutoff of 20.75 and the 2400 Å sample selected at observed U with a cutoff of 24.0.

These calculations are stringent tests of our SED model and sample characterization. The SED model is used with the mean SED parameters of the various galaxy spectral groupings from Table 3 of Cohen (2001) to convert between rest-frame luminosity and observed magnitudes. This is required to determine the low-luminosity cutoff at a particular rest-frame wavelength of the integral for the predicted comoving number density (and also the integral for the predicted mean observed luminosity of the sample). A small error in this value will produce, for galaxy spectral groupings with steep faint-end slopes, a substantial error in the prediction [$\sim 30\%$ for a 0.2 mag error in M(cutoff)].

The results are presented in Table 14. As expected, the LFs derived here predict the observed galaxy counts to $R = 23.5$ mag to within $\sim 30\%$ throughout. The agreement is particularly good for galaxy spectral groups with less steep faint-end slopes.

Also illustrative is a calculation of the predicted mean $L(R)$ for the sample of galaxies observed. This calculation too is a stringent test of our SED model as the same procedure to define the lower limit in the integration for the predicted mean $L(R)$ for the number densities is used here as well. We adopt the same cutoffs as above for the observed U-, R-, and K-selected samples. The results are given in Table 15. The entry in Table 15 for the group of "all" galaxies includes both the observed and predicted values for the mean value of the rest-frame luminosity for the observed sample. These are in reasonable agreement throughout.

The predicted values in Table 15 show the expected very strong increase with redshift as the less luminous galaxies drop out of the magnitude-limited sample toward higher z.

TABLE 15

MEAN PREDICTED REST-FRAME LUMINOSITY OF OBSERVED SAMPLE[a]

Galaxy Types	$z < 0.25$ $L(R)(10^{36}$ W)	$0.25 < z < 0.5$ log $[L(10^{36}$W)]	$0.5 < z < 0.8$ log $[L(10^{36}$W)]	$0.8 < z < 1.05$ log $[L(10^{36}$W)]	$1.05 < z < 1.5$ log $[L(10^{36}$W)]
			Rest-Frame U		
$\mathscr{A}$	...	4.8	8.2	16.1	...
$\mathscr{I}$	...	4.2	6.0	...	...
$\mathscr{A} + \mathscr{I}$	...	4.2	6.8	14.9	...
$\mathscr{I} + \mathscr{E}$	...	2.4	3.3	6.8	...
$\mathscr{E}$	...	1.3	2.3	6.5	...
All (predicted).....	2.0	3.6	4.2	7.5	20.9
All (observed)	1.0	2.1	3.9	7.2	20.0
			Rest-Frame R		
$\mathscr{A}$	...	6.5	14.5	29.0	...
$\mathscr{I}$	...	5.2	12.0	...	...
$\mathscr{A} + \mathscr{I}$	...	6.0	12.0	25.5	...
$\mathscr{I} + \mathscr{E}$	...	4.4	5.4	11.9	...
$\mathscr{E}$	...	1.6	2.9	10.6	...
All (predicted).....	1.0	4.3	7.7	14.2	26.9
All (observed)	1.3	3.7	7.1	11.6	17.8
			Rest-Frame K		
$\mathscr{A}$	...	3.6	11.3	16.5	...
$\mathscr{I}$	...	3.0	5.4	13.5	...
$\mathscr{A} + \mathscr{I}$	...	3.1	7.5	16.9	...
$\mathscr{I} + \mathscr{E}$	...	2.1	2.8	3.7	...
$\mathscr{E}$	...	0.8	1.4	4.4	...
All (predicted).....	1.4	2.5	4.3	6.7	10.0
All (observed)	0.7	2.1	3.6	5.5	6.7
			Rest-Frame 2400 Å		
$\mathscr{I}$	...	1.7	3.0	...	...
$\mathscr{A} + \mathscr{I}$	...	1.6	2.8	9.0	...
$\mathscr{I} + \mathscr{E}$	...	1.4	2.7	5.5	...
$\mathscr{E}$	...	1.3	2.5	5.2	...
All (predicted).....	...	1.4	2.6	5.6	9.5
All (observed)	...	1.0	2.3	4.7	7.3

[a] This is the predicted mean luminosity of a sample observed to our limiting magnitude, calculated to a cutoff of R(observed) = 23.5 and K(observed) = 20.75. See Table 16 for the luminosity density.

Because of the steep faint-end slope of the LF for the galaxies with strong emission lines, their mean $L(R)$ within our sample increases by a factor of ~ 5 between $\langle z \rangle = 0.4$ and 0.9 while the mean luminosity of the sample's absorption-line galaxies is predicted to increase only by a factor of ~ 3.

8. THE LUMINOSITY DENSITY AND ITS EVOLUTION WITH REDSHIFT

We compute the luminosity density between $10L^*$ and $L^*/20$ by integration using the parameters of the best-fit LF at each rest-frame wavelength and for each galaxy spectral grouping. The resulting values for $\rho(L)$ using α and L^* from the two-parameter Schechter fits are given in Table 16. Appendix B, where a different set of assumptions are made to analyze our sample, establishes that these values for $\rho(L)$ are very robust. Note that these tabulated values must still be corrected for the various selection issues described in § 7.2, such as the disappearance of $\mathscr{A}$ galaxies from the sample as they become EROs. We have not tried to adjust α for each of the different rest-frame wavelengths to be identical for each galaxy spectral group; they are consistent to within the uncertainties, but not identical.

For rest-frame R and K, we give 1 σ errors as a percentage of $\rho(L)$. These were calculated utilizing the 1 σ error contours of the two-parameter LF solutions. We take the L^* and α from these contours at the ends of the major and minor axes of the error contour. We then propagate these values through the codes to calculate four values of ϕ^* and $\rho(L)$. We take the average of the absolute values of the fractional deviations with respect to the nominal value as the 1 σ error. This is an approximation for the true σ but should be close enough for our purposes, given our small sample size. Error estimates for ϕ^* can be calculated in a similar manner but are not very useful as α is varying between the points selected on the error contour, hence the results are not directly comparable.

We use the three-parameter simultaneous fits for α, L^*, and Q, when available, to generate Figure 11, which shows the evolution of the luminosity density from 0.24 to 2.2 μm in the rest frame for the $\mathscr{A}$ and the $\mathscr{I} + \mathscr{E}$ galaxy spectral groupings (*filled and open circles*, respectively), as well as for the group of all galaxies, indicated by the larger symbols. A correction for galaxies missing from the sample calculated from the number densities in the relevant tables (e.g., Table

TABLE 16

LUMINOSITY DENSITY AT REST-FRAME 2400 Å, U, R, AND K ($10L^*$ TO $L^*/20$)

GALAXY TYPES	ρ (10^{34} W Mpc^{-3}) $z = 0.01$–0.25	$z = 0.25$–0.5	$z = 0.5$–0.8	$z = 0.8$–1.05	$z = 1.05$–1.5
		Rest-Frame U			
$\mathscr{A}$	...	0.9	1.7	1.6	...
$\mathscr{I}$	...	2.9	1.8	...	...
$\mathscr{A} + \mathscr{I}$	...	3.6	3.5	2.4	...
$\mathscr{I} + \mathscr{E}$	...	3.8	3.3	5.5	...
$\mathscr{E}$	...	1.2	1.6	4.9	...
All	≥ 4.2	3.8	4.9	6.9	1.0[a]
		Rest-Frame R			
$\mathscr{A}$	...	1.2 (± 48)	2.9 (± 29)	2.2 (± 28)	...
$\mathscr{I}$	...	3.5 (± 26)	2.9 (± 29)	...	...
$\mathscr{A} + \mathscr{I}$	...	5.2 (± 22)	6.6 (± 18)	3.5 (± 35)	...
$\mathscr{I} + \mathscr{E}$	...	7.2 (± 19)	5.1 (± 18)	9.3 (± 12)	...
$\mathscr{E}$	...	2.0 (± 29)	2.3 (± 39)	8.1 (± 10)	...
All	≥ 1.9 (± 55)	7.7 (± 17)	8.6 (± 14)	11.5 (± 16)	0.9[a]
		Rest-Frame K			
$\mathscr{A}$	...	0.7 (± 66)	2.0 (± 36)	1.4 (± 42)	...
$\mathscr{I}$	...	2.2 (± 27)	1.7 (± 24)	0.9 (± 98)	...
$\mathscr{A} + \mathscr{I}$	...	2.8 (± 23)	3.7 (± 18)	2.4 (± 36)	...
$\mathscr{I} + \mathscr{E}$	...	3.3 (± 30)	2.6 (± 19)	3.7 (± 14)	...
$\mathscr{E}$	...	0.7(± 43)	0.9 (± 15)	2.8 (± 17)	...
All	≥ 2.2 (± 66)	4.4 (± 27)	4.6 (± 17)	5.0 (± 15)	0.5[a]
		Rest-Frame 2400 Å			
$\mathscr{A}$	...	...	0.2	...	...
$\mathscr{I}$	...	1.1	0.9	...	...
$\mathscr{A} + \mathscr{I}$	...	1.2	1.0	0.4	...
$\mathscr{I} + \mathscr{E}$	...	2.1	2.3	3.5	...
$\mathscr{E}$	...	1.0	1.4	3.2	...
All	...	2.2	2.4	3.5	0.8[a]

NOTE.—Values in parentheses are in %.

[a] The values for the bin $1.05 < z < 1.5$ are suspected to be underestimated by substantial factors whose approximate values are given in the text. See the text for details.

5 and its equivalent at other rest-frame wavelengths) has been applied to the highest redshift bin $1.05 < z < 1.5$ and to the group of $\mathscr{A}$ galaxies for $0.8 < z < 1.05$, where they drop out of the sample as well. This correction for the highest redshift bin is large (a factor of 3–10) and uncertain.

Overall, we see a slow increase in the luminosity density, with the increasing fractional contribution of the $\mathscr{A}$ galaxies at redder rest-frame wavelengths, as expected. Correcting for the loss of $\mathscr{A}$ galaxies from the sample in the highest redshift bins, Figure 11 suggests that the fractional contribution by the various galaxy groupings does not change much with redshift for a particular rest wavelength, at least over the redshift regime considered here.

8.1. *The Star Formation Rate and Its Dependence on Redshift*

The flux in the UV continuum of galaxies is often used as an indicator of the star formation rate (SFR), along with emission at Hα, the λ3727 line of [O II], other photoionized optical emission lines, as well as radio emission. For $z > 0.25$ we observe the mid-UV directly from the ground for the galaxies in our sample.

We have computed the luminosity density at 2400 Å from the data in our redshift survey. There are three places relevant quantities appear in the tables. The first is Table 10, where L^*(2400 Å) is seen to be rising rapidly with redshift for the $\mathscr{E}$ spectral grouping and for all the galaxies together. This gives rise to the entries for rest-frame 2400 Å in Table 12 which are computed directly from the above and hence also indicate a rapid rise in L^*(2400 Å) of a factor of 5–10 between $z = 0$ and 1. The global solution for Q given in Table 13 also suggests a brightening in L^*(2400 Å) by a factor of 10 over this redshift interval. This value is in agreement with the rapid increase in total emission in the [O II] λ3727 emission line found by Hogg et al. (1998) and Lilly et al. (1996) and disagrees with the value smaller by about a factor of 3 found by Cowie, Songaila, & Barger (1999), who analyzed part of the present sample together with additional data from the Hawaii Deep Fields to deduce the UV luminosity density.

The luminosity density calculations for rest-frame 2400 Å are given in Table 16, and at $0.25 < z < 0.5$ they are very close to that determined recently for the local universe by Treyer et al. (1998). The values in Table 16 support an

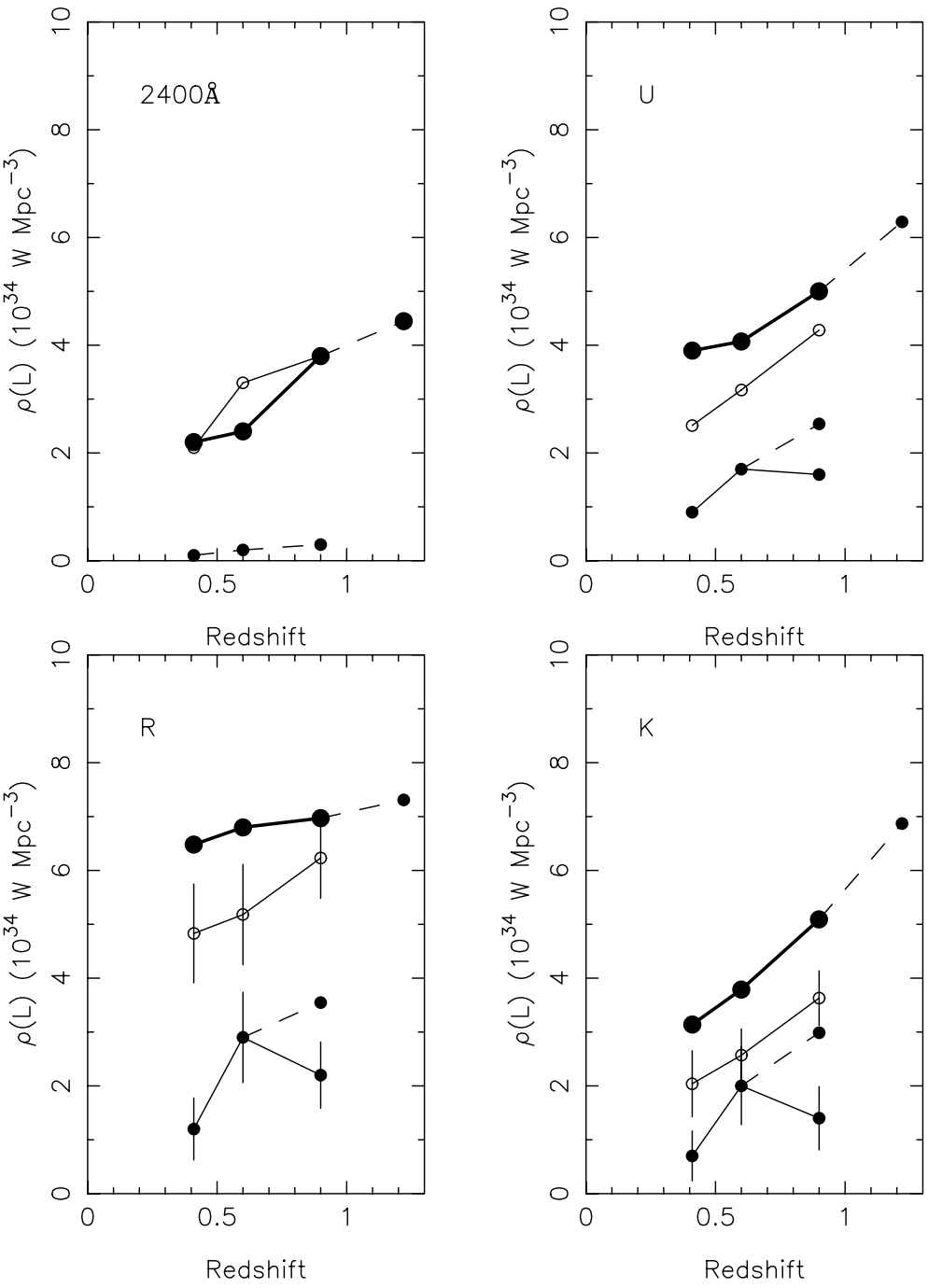

FIG. 11.—Evolution of the luminosity density with redshift shown for four rest-frame wavelengths from 0.24 to 2.2 μm for the $\mathscr{A}$ galaxies (*filled circles*), $\mathscr{I} + \mathscr{E}$ galaxies (*open circles*), and the group of all galaxies (*larger filled circles*); 1 σ errors are shown for R and K only. The three-parameter solutions have been used when available. Corrections have been applied for galaxies missing from the sample for the highest redshift bin and for the $\mathscr{A}$ galaxy grouping in the bin $0.8 < z < 1.05$ only. Dashed lines connect such corrected points.

increase in $\rho(L)$(2400 Å) with redshift as well, but by a somewhat smaller factor. As shown in Figure 11, the increase in $\rho(L)$ at 2400 Å corresponds to $Q \sim 0.6$, i.e., a factor of 4 increase of $\rho[L(2400\ \text{Å})]$ at 2400 Å between $z = 0$ and 1.

Because of the strong negative covariance between α and L^*, any estimate of the UV luminosity density based solely on values of L^* which ignores completely the role of α must be viewed with suspicion. Hence, we prefer the estimate for the change of the UV luminosity density with redshift based on the appropriate integrations for $\rho[L(2400\ \text{Å})]$ described above, whose results are given in Table 16 and Figure 11. These suggest that $\rho[L(2400\ \text{Å})]$ increases by a factor of ~ 4 between $z = 0$ and 1. However, given the current controversy over this issue and its overall importance, we are planning to redo the measurement of the λ3727 line strengths shortly as this should provide a more definitive value for the SFR and one potentially less affected by extinction than a value based on the UV luminosity density. Our preliminary analysis of the spectra suggests that the mean rest-frame equivalent width of the λ3727 emission line of [O II] for our observed sample of galaxies in the region of the HDF remains approximately constant with redshift,

which requires the mean observed equivalent width to increase $\propto(1+z)$. Under these circumstances, the emitted flux in this emission line will increase substantially with redshift as a result of the substantial rise in mean luminosity of the observed sample given in Table 15. This issue will be discussed at length in the next paper in this series.

9. COMPARISON WITH GALAXY EVOLUTION MODELS

Once a model for the evolution of the integrated light for a galaxy is adopted, a number of other calculations become feasible. We can, for example, extrapolate the luminosity densities in each redshift bin given in Table 16 into luminosity densities at $z = 0$, taking out the expected trends due to normal stellar evolution. This is straightforward for galaxies with little star formation. For galaxies with considerable star formation during the time (redshift) interval in question, assumptions regarding the form of the SFR as a function of z become more critical. We adopt the galaxy evolution models of Poggianti (1997) for this purpose. In particular, her elliptical model has an initial burst of star formation with an exponential decay timescale of 1.0 Gyr and is 15 Gyr old. Her model for Sc galaxies assumes an SFR proportional to the gas fraction and includes inflow.

Quiescent galaxies within which significant star formation has not occurred during the entire redshift range spanned here will basically be fading in luminosity strictly through stellar evolution. The detailed behavior of the fading as a function of redshift and rest-frame wavelength depends only on the adopted stellar evolutionary tracks and on the conversion between time and redshift (the cosmology). They are seen as $\mathscr{A}$ galaxies throughout the sample volume. In actively star-forming galaxies, on the other hand, the fading with time from passive stellar evolution, although always occurring, can be overcome by the additional luminosity input from young stars.

Figure 12 compares the luminosity evolution we find for the region of the HDF given in Table 13 (*filled circles*) with those predicted from the model. The mean redshifts of the three bins between $z = 0.25$ and 1.05 are used, and the points represent L^* for rest-frame U, R, and K for $\mathscr{A}$ and $\mathscr{I}+\mathscr{E}$ (i.e., relatively quiescent and star-forming) galaxies. These points are connected by the solid lines. The three-parameter solution for Q is used. Because here we are focusing on L^* only, the luminosities in each of the rest-frame bands have been shifted to the value of α obtained for rest-frame R for each galaxy spectral grouping. This requires adding a small constant offset to the result for log L^* in each redshift bin. The constant is different for each galaxy spectral grouping and also varies with rest-frame wavelength. (It is 0 at rest-frame R.) The predictions of Poggianti's models in this figure are represented by the open circles, which for each rest-frame color are connected by dashed lines.

The agreement between the evolution in L^* with redshift as a function of rest-frame color that we derive through our analysis of the LF for galaxies in the region of the HDF and that predicted by Poggianti's (1997) galaxy synthetic spectral evolution models for the Sc model with the star-forming galaxies in our sample is reasonable at all rest-frame wave-

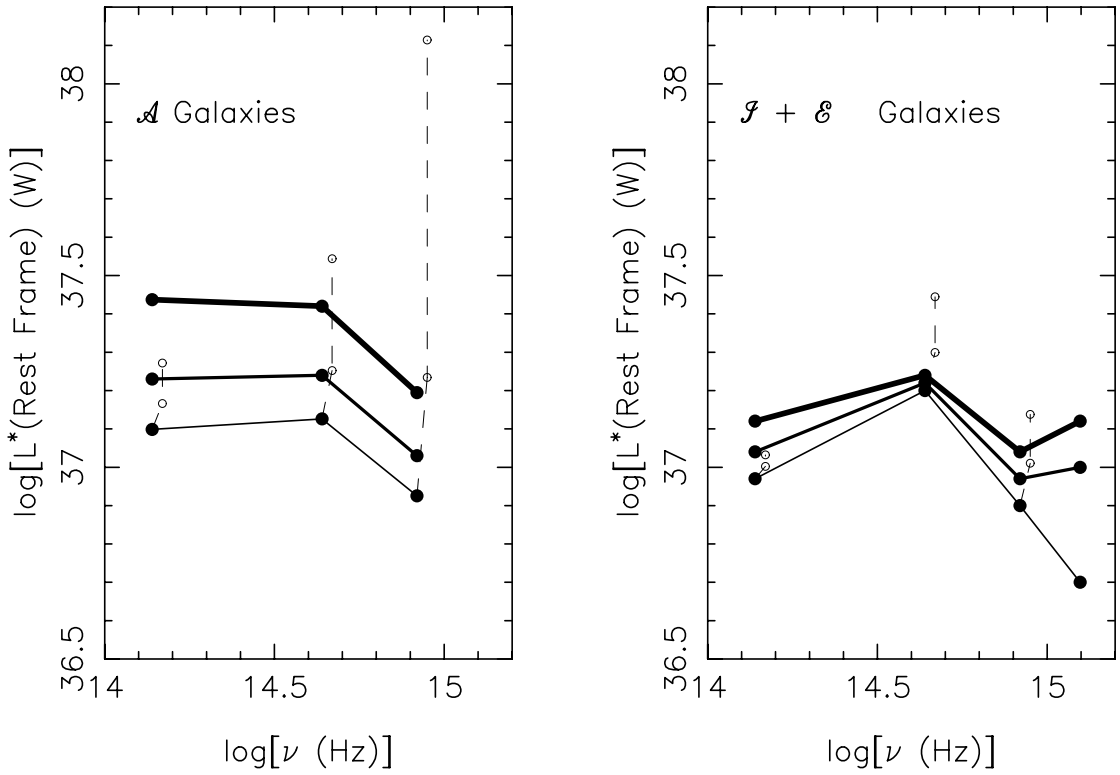

FIG. 12.—Evolution of an L^* galaxy in rest-frame U, R, and K with redshift. The filled circles represent the values computed from Table 9 for absorption-line galaxies (*left panel*) and emission-line galaxies (*right panel*). The α determined from rest-frame R is used throughout. The results of the three redshift bins covering the range $0.25 < z < 1.05$ are shown, with the lines becoming thicker as the redshift of the bin increases. The results at rest-frame 2400 Å are shown only for the emission-line galaxies. The open circles (connected by dashed lines) are the predicted evolution for an elliptical with an initial star formation burst with a duration of 1 Gyr and an age of 15 Gyr at present and for an Sc galaxy with an SFR dependent on gas density as predicted by Poggianti (1997).

lengths. The agreement for the more quiescent galaxies is fair at R and K but poor at rest-frame U. The passively evolving model predicts a fading at rest-frame U with increasing time that is significantly larger than that inferred by our analysis. The predicted fading of ~ 0.9 dex in $\log [L^*(U)]$ between $\langle z \rangle = 0.9$ and 0.6 is not present in the data.

One cannot argue that these galaxies at $z \gtrsim 0.5$ are masquerading as galaxies of any other spectral group as they remain very red in the rest-frame optical/near-IR. Such red galaxies very rarely, if ever, show emission lines throughout the relevant redshift range (see Cohen 2001) and hence have little or no current star formation until beyond $z = 1.5$. They therefore cannot have morphed out of the $\mathscr{A}$ galaxy group.

It is undoubtedly true that an adjustment to the star formation prescription used by Poggianti to generate the SED of the quiescent galaxies could resolve these problems. The general form required is for a small tail of residual star formation to continue with time beyond the initial burst.

At our request, B. M. Poggianti (2001, private communication) has recalculated the evolutionary corrections for the $\mathscr{A}$ galaxies using our cosmology and also changing the e-folding time of the initial burst from 1 to 0.5 Gyr. The values published in Poggianti (1997) are recovered with the appropriate inputs. However, the new evolutionary corrections at rest-frame U are much smaller at high z than those published in Poggianti (1997). For example, at $z = 1$, the new evolutionary correction is ~ 2.5 mag smaller. These new evolutionary corrections provide a much better fit to our results.

Figure 12 recovers one of the key results of Cohen (2001), that the major change in galaxy SEDs with increasing redshift in this redshift range is the rest-frame UV becoming bluer for actively star-forming galaxies. Here we add an evaluation of the trend of overall luminosity.

9.1. *Total Stellar Mass in Galaxies as a Function of Redshift*

One rationale for studying galaxies at K is that the integrated light there is much more representative of the total stellar mass of a galaxy than are the optical colors, where light from the most recent epoch of star formation involving only a small fraction of the stellar mass in the galaxy may dominate over that from the much more massive older population as one moves toward the UV. To convert the rest-frame K luminosity density that we measure as a function of redshift (given in Table 16) into total stellar masses of the galaxies requires a model of evolving galaxy SEDs to evaluate their mass-to-light ratio as a function of look-back time and of their star formation history. Because the evolutionary corrections at K are small and almost independent of spectral type over the range of stars that contribute substantially to the integrated light of a galaxy at this rest-frame wavelength, we are able to accomplish this transformation with some degree of precision and hence to deduce the total stellar mass in galaxies as a function of redshift. Any variation in the total stellar mass must be a result of star formation.

We use the models of Poggianti (1997) for the evolution of galaxy integrated light to extrapolate the luminosity densities at rest-frame K, $\rho(L/K)$ at z_i, given in Table 16 to values at $z = 0.0$, $\rho(L/K/z_i$ at $z = 0.0)$, so that they can be directly compared. This quantity is then converted into total stellar mass in galaxies assuming that a constant mass-to-light ratio at rest-frame K applies to all galaxies at $z = 0.0$; we adopt 0.8 (in solar units).

TABLE 17

LUMINOSITY DENSITY AND STELLAR MASS AT REST-FRAME K EXTRAPOLATED TO $z = 0.0$

GALAXY TYPES	ρ[a] (10^{34} W Mpc^{-3})[b]		
	$z = 0.25$–0.5	$z = 0.5$–0.8	$z = 0.8$–1.05
$\mathscr{A}$	0.49 ($\pm$65)	1.19 ($\pm$39)	0.65 ($\pm$44)
$\mathscr{I}$	1.31 ($\pm$31)	0.93 ($\pm$28)	0.38 ($\pm$98)
$\mathscr{I} + \mathscr{E}$	2.31 ($\pm$36)	1.58 ($\pm$22)	1.93 ($\pm$20)
$\mathscr{E}$	0.56 ($\pm$24)	0.64 ($\pm$21)	1.82 ($\pm$20)
Total [$\mathscr{A} + (\mathscr{I} + \mathscr{E})$].....	2.80 ($\pm$32)	2.77 ($\pm$20)	2.58 ($\pm$19)

NOTE.—Values in parentheses are in %.

[a] Integrations go from $10L^*(z)$ to $L^*(z)/20$.

[b] Note that 1.0×10^{34} W Mpc$^{-3} \equiv 1.3 \times 10^8 L_\odot$ Mpc$^{-3} \equiv 1.6 \times 10^8 M_\odot$ Mpc^{-3}.

The results are given in Table 17. The entries in the table are given in the form of $L(K/z)$ extrapolated back to $z = 0$ in units of W Mpc^{-3}. The conversion factors required to obtain values in units of $L_\odot$ Mpc^{-3} or $M_\odot$ Mpc^{-3} are given in the notes to the table. The uncertainties have been propagated using the values from Table 16 for K and assuming a 15% uncertainty in the evolutionary correction that brings the observed $L(K/z)$ back to $z = 0$. If the contribution of the different galaxy spectral groupings to the integrated light at K were constant with z, the M/L adopted would act strictly as a normalization factor. Hence, we ignore its uncertainty in this calculation.

There is no sign in Table 17 of any substantial increase in the total mass in stars between $z = 0.25$ and 1.05. The total stellar mass in galaxies appears to be constant with redshift to within $1\sigma = \pm 20\%$. This statement is not inconsistent with the claim made above in § 8 that the UV luminosity density at 2400 Å and hence the SFR are increasing substantially between $z = 0$ and 1. If we adopt the conversion between UV flux and SFR given by Kennicutt (1998) and integrate the UV luminosity density $\rho(L/2400$ Å) as a function of time between the present and $z = 1.05$, we find that $\lesssim 20\%$ of the total stellar mass currently in galaxies given in Table 17 has been formed since $z = 1.05$, depending on the exact choice of Q for rest-frame 2400 Å and on the mean extinction adopted.

10. CHANGING THE COSMOLOGY

Since the key parameters are proportional to H_0^n ($n = 2$ for L, $n = 3$ for the comoving number density, and $n = 1$ for the comoving luminosity density), the consequences of changes in H_0 are easily evaluated. The effect of the choice of Ω and Λ is more subtle, as both the luminosity distance ($L \propto D_L^2$) and the cosmological comoving volume, which affects comoving densities, are nonlinear in these parameters. We compare the result of adopting the flat model $\Omega_m = 0.3$ and $\Lambda = 0.7$ suggested by the cosmic microwave background fluctuation measurements (de Bernardis et al. 2000) instead of the model adopted in this series of papers, $\Omega_m = 0.3$, $\Lambda = 0$, which has the virtue that many cosmological quantities of interest have analytical solutions.

The luminosity distance for the flat model is $\sim 8\%$ larger than it is for the model we use, which is a difference that can

be removed by modifying the adopted value of H_0 from 60 to 65 km s^{-1} Mpc^{-1}. More importantly, the ratio of luminosity distances between the two models changes as a function of z by only about 10% over the range $z = 0.25$–1.5, with the flat model having luminosity distances that increase more rapidly with redshift. Adoption of such a model would mean that the more distant galaxies in our sample would become slightly brighter by $\sim$0.07 dex in log L compared to the nearest galaxies. These small changes are well within our errors. Given the contribution from passive stellar evolution within galaxies, which is larger than this cosmological difference, there is no hope of using our sample to learn anything about cosmology.

In the flat model with $\Omega_m = 0.3$, the differential comoving volume between redshift z and $z + \Delta(z)$, $V(z)$, is larger for the flat model than for the cosmological model we use here. Moreover, $V(z)$ for the flat model increases even more rapidly at high redshift than does $V(z)$ for the cosmology adopted here: $[V(z = 1.0)/V(z = 0.3)$ for $\Omega_m = 0.3$, $\Lambda = 0.7]/[V(z = 1.0)/V(z = 0.3)for\Omega_m = 0.3$, $\Lambda = 0.0] = 1.23$ for $\Delta(z) = 0.10$. This difference exacerbates the problems of the low comoving density we have inferred in our analysis for $z > 1.1$ in § 7. A larger survey with better understanding of the sample completeness for $z > 1$ might be sensitive to this difference in comoving volume.

11. COMPARISON WITH THE RESULTS OF OTHER SURVEYS

In comparing our characteristic luminosities with those of other surveys, we convert the cosmology to that adopted here.[4] We also report two values of L^*. The first is that obtained from the maximum likelihood solution with fixed α given in the appropriate one of Tables 5, 7, 8, or 10 for the $z = 0.25$–0.5 bin. This value is then extrapolated to $z = 0.0$ (for comparison with local surveys) using the values for Q from Table 13. Since all local redshift surveys have much larger galaxy samples than we do, we assume that their determinations of the faint-end slope of the LF are correct. Therefore, a second comparison value is obtained from our tables by finding L^* at the value of α of the local survey, which may not be the same as our best value of α of Table 11. Because of the covariance between L^* and α, this second value of L^* is perhaps the most valid for the comparison. Values of α are directly comparable; no adjustments are required.

Local surveys determine the LF over a much wider range of luminosity than is possible when very distant galaxies are involved. Their luminosity density integrals are carried out to fainter lower limits in $L(R)$, and their total luminosity densities are correspondingly higher. To overcome this, we assume that all published local measurements go to much fainter luminosities relative to L^* than do ours and that they should be corrected by the ratio appropriate to a Schechter function for the relevant value of α,

$$\frac{\Gamma(\alpha + 2)}{\int_{0.05}^{10} (L/L^*)\phi(L/L^*)d(L/L^*)}.$$

Table 18 gives the details for all the comparisons described below. In all such comparisons, one must remember that different survey teams adopt slightly different definitions for their galaxy spectral groupings.

11.1. *Comparison with Local Values for α and for $L^*(R)$*

The Las Campanas Redshift Survey (LCRS; Shectman et al. 1996), with $\sim$20,000 galaxies with a mean z of 0.10, was the first local redshift survey big enough to ensure that the LF determination would be highly accurate. Lin et al. (1996) carried out the LF analysis in the (pseudo-)R band of that survey. They find $\alpha = -0.70$ and, adjusting to our cosmology, as we do for all such comparisons, log $[L^*(R)] = 36.76$ dex, including a small (0.1 mag) factor to convert between the R-band photometric system of the Canada-France Redshift Survey (CFRS) and ours. Separating the sample into emission-line and non–emission-line objects, dividing at an equivalent width of 5 Å for the λ3727 line of [O II], Lin et al. (1996) found variations of the faint-end slopes and characteristic luminosities shown in Figures 9 and 10 and given in Table 18. In Figure 10 we also superpose the predicted passive stellar evolution for an elliptical and for an Sc galaxy from Poggianti (1997), indicated by the thin solid curves. These have an arbitrary vertical zero-point offset, which was set for convenience here.

Blanton et al. (2001) report the preliminary LF from the Sloan Digital Sky Survey (SDSS) for more than 11,000 galaxies for five rest-frame bands 3560–9130 Å. Applying the conversion factor between various R-band observational systems recommended by Fukugita et al. (1996) leads to $L^*(R) = 37.01$, with $\alpha = -1.16$. It is very interesting that the faint-end slope for the sample as a whole does not vary noticeably over this wavelength range; ours does not either, at least between 0.36 and 2.2 μm in the rest frame.

Initial results for the 2dF survey were presented in Folkes et al. (1999) in the b_j band. Now that the 2dF galaxy redshift sample is in excess of 45,000, Cross et al. (2001) provide an update on the galaxy LF, with improved photometry, and they introduce a more complex bivariate form for the LF. They deduce, for the entire sample, converting their photometry into R using the mean color of galaxies from Fukugita et al. (1996), a value of $L^*(R)$ identical to within $\pm$0.02 mag that of Blanton et al. (2001) with $\alpha = -1.09$. These large surveys provide a local calibration of the LF to which our data are compared in Table 18.

Our value of log $[L^*(R)(W)]$ at $z = 0.0$ from the three-parameter fit using all galaxies is 37.20 dex. When corrected to the same value of α as the 2dF results, this becomes log $[L^*(R)(W)] = 36.96$, in good agreement with their values for L^*. Overall the agreement shown in Table 18 is reasonably good considering that a double extrapolation of our L^* values is often required, once in redshift and again in α, to obtain the entries given in the last column. Our value of α (-1.10 ± 0.10) for the entire sample is in excellent agreement with these local measurements.

Given the high-precision photometry possible for bright extended nearby galaxies, Blanton et al. (2001) have carefully analyzed the best way to extrapolate to true total galaxy brightness measurements within very large radii. They claim that total galaxy luminosities were underestimated by a factor of 2 by the LCRS survey through use of the isophotal aperture photometry adopted by the LCRS group. However, the luxury of a complex analysis using Petrosian (1976) magnitudes is beyond our reach with such faint galaxies and ones so distant that spatial resolution is very limited.

[4] In practice, we just adjust for any difference in the adopted values of H_0.

TABLE 18

COMPARISON WITH LF PARAMETERS OF OTHER SURVEYS

Reference	Galaxy Types	log [$L^*(W)$]	α	log [$L^*(W)$]	α (CFGRS)	log [$L^*(W)$] (adjusted α)[a]
Rest-Frame R	Local	...	...	...	...	...
LCRS.....	All	36.76 ± 0.02	-0.70 ± 0.03	37.20	-1.30	36.65
	Emission	36.66 ± 0.04	-0.90 ± 0.10	36.71	-1.45	36.15
	No emission	36.74 ± 0.04	-0.27 ± 0.10	36.92	-0.50	36.60
SDSS	All	37.01 ± 0.02	-1.20 ± 0.03	37.20	-1.30	37.09
2dF	All	37.00 ± 0.02	-1.09 ± 0.09	37.20	-1.30	36.96
	Emission	36.70 ± 0.04	-1.70 ± 0.10	36.71	-1.45	37.07
	No emission	36.95 ± 0.05	-0.70 ± 0.10	36.92	-0.50	37.13
Rest-Frame K	Local	...	...	...	...	...
Cole et al. (2001)	All	36.89 ± 0.02	-0.96 ± 0.05	36.80	-1.25	36.60
Kochanek et al. (2001).....	Early	36.92 ± 0.03	-0.90 ± 0.10	36.30	-0.10	37.00[c]
	Late	36.70 ± 0.03	-0.90 ± 0.10	36.10	-1.35	35.60
			Intermediate z			
CNOC2	$\langle z \rangle = 0.3$	...	...	...	...	...
Rest-Frame R	Early	36.84 ± 0.05	-0.06 ± 0.14	36.86	-0.50	36.56
	Late	36.68 ± 0.06	-1.34 ± 0.12	36.65	-1.45	36.52
Rest-Frame U	Early	35.93 ± 0.05	0.14 ± 0.15	36.23	-0.35	36.03
	Late	36.25 ± 0.05	-1.14 ± 0.15	36.66	-1.60	36.26
CFRS.....	$\langle z \rangle = 0.56$	...	...	...	...	...
Rest-Frame B.....	All	36.62	-0.50	37.15	-1.15	36.35[c]
	Red	36.69	-0.37	37.14	-0.50	37.01
	Blue	36.82	-1.07	36.79	-1.05	36.79
			High z			
Steidel et al. (1999).....	$z \sim 3$	...	...	...	...	...
Rest-Frame 1500 Å	LBG	37.59 ± 0.06	-1.60 ± 0.13	36.75[b]	-0.60	37.15[c]

[a] Here the value of L^* is adjusted so that the value of α(CFGRS) matches that of the comparison survey.
[b] L^* at rest-frame 2400 Å for galaxies at $z \sim 1.3$.
[c] A very large extrapolation in α is required. The resulting L^* is quite uncertain.

11.2. *Comparison with Local Values for $L^*(K)$*

Cole et al. (2001) utilize the current overlap of the 2MASS (Skrutskie et al. 1997) all-sky infrared photometry campaign and the 2dF redshift survey to find that $M^*(K_S) = -23.44$ and $\alpha(K_S) = -0.9$ for $H_0 = 100$ km s^{-1} Mpc^{-1} from a sample of $\sim$17,000 galaxies. This translates into log [$L^*(K)$] = 36.88 dex for $H_0 = 60$ km s^{-1} Mpc^{-1}. Kochanek et al. (2001) do the same for the $\sim$4100 galaxies in common between 2MASS and the CfA "z-cat" redshift catalogs of nearby galaxies. They find that galaxies of different spectral types all have the same faint-end slope $\alpha \sim -0.9 \pm 0.1$ but that M^* varies from -23.0 to -23.5, being brighter for earlier morphological types. Note that Marzke et al. (1994) have shown that the CfA survey, when divided on the basis of galaxy morphology, also yields LFs at B whose faint-end slopes are indistinguishable among the various subsamples, except for the Sm–Im galaxies, which show a much steeper faint-end slope, but whose presence will be minimal in K-selected samples of nearby galaxies.

11.3. *Comparison with Previous Results for Intermediate Redshift*

The largest surveys including at least part of the redshift range discussed here are the CNOC2 survey and the CFRS. The CNOC2 survey (Yee et al. 2000) covers the regime $0.12 < z < 0.55$ and $17 < z < 21.5$ with $\langle z \rangle \sim 0.3$ and contains about 2000 galaxies in four separate fields. The LF analysis is given in Lin et al. (1999). Redshifts are only available for a subset of these; SED parameters from their multicolor photometric database are used to infer the redshifts of the remaining objects. They use three SED-based galaxy spectral classes, early, late, and intermediate, and calculate the LF in the rest-frame U, B, and R bands. They established that within this regime, the early- and intermediate-type galaxies primarily show brightening at higher redshift, with only modest density evolution, while the late-type galaxies show little luminosity evolution and strong density evolution. The typical value of Q they find for their early-type galaxies corresponds to $\sim$0.6, while for late-type galaxies it is $\sim$0.1, which are quite comparable to the values we derive given in Table 9.

Our results are in good agreement with their conclusions regarding early-type galaxies (which we call $\mathscr{A}$ and $\mathscr{I}$ galaxies), extending them significantly higher in redshift. However, we find little density evolution among the late-type galaxies, with moderate luminosity evolution.

The values for the faint-end slope of the LF given by Lin et al. (1996) are roughly independent of redshift between their three bands (U to R) and are quite consistent with the values we derive given in Table 11. The quantitative agreement between our LF parameters and those determined by the CNOC2 survey is quite good as is shown in Figures 6 and 7 and Table 18.

The total luminosity density of the CNOC2 survey at rest-frame R, with a mean z of 0.3, is about 13.8×10^{34} W

Mpc^{-3}. When we correct our value of 7.7×10^{34} W Mpc^{-3} by the appropriate factor to compensate for the difference in the lower luminosity limit of the integration between the CNOC2 survey and our work, we obtain excellent agreement, to within $\sim 10\%$.

The CFRS is described in Le Fèvre et al. (1995). It contains 730 galaxies, of which 591 have spectroscopic redshifts with median $z = 0.56$ within five fields with $17.5 < I < 22.5$. The LF analysis of the CFRS is presented in Lilly et al. (1995). They divide their sample into two galaxy groups, "red" and "blue," and solve for the rest-frame B luminosity evolution. Here we do not agree as well with regard to the evolution of the LF. As shown in Figures 9 and 10, the CFRS tends to have LF solutions that run away as z increases toward steeper faint-end slopes, which in turn requires very bright L^* values. While there are probably no galaxies so luminous in the data, the fit is not rejected because the LF becomes so steep that the probability of seeing them becomes very low. Our solutions do not show such extreme ranges in α for a given galaxy spectral grouping, and thus we avoid the extremely high L^* values which they find in their highest z bins. As Lilly et al. (1995) state, because of the high coupling between the LF parameters, the values they tabulate of these parameters should not be taken in isolation but rather viewed together as the evolution of the LF, and in that spirit our results can be viewed as being in somewhat better agreement.

We have not carried out an analysis at rest-frame B. The comparison shown in Figure 10 assumes that $\log [L^*(B)(W)]$ at $z = 0.6$ is equivalent to $\log [L^*(R)(W)] = 37.2$ dex, while the conversions given in Table 18 approximate $L^*(B)$ from our results by using $0.5[L^*(U) + L^*(R)]$. The comparison given in the table is from a redshift regime ($z \sim 0.6$) just before the CFRS LFs start becoming unexpectedly bright as described above.

The luminosity density, since it is an integral over the LF, is a more robust measure to compare than the individual parameters that are used to characterize the LF. We evaluate the total luminosity density for the CFRS as a function of redshift range and galaxy spectral grouping by integrating the LFs between $10L^*$ and $L^*/20$ using the parameters (α, L^*, and ϕ^*) specified by the CFRS. We convert our results from Table 16 using the procedure above to derive rest-frame B values. The total luminosity density of the CFRS survey at rest-frame B, with a mean z of 0.3, is about 7.3×10^{34} W Mpc^{-3}, which is very close to the value 6.8×10^{34} W Mpc^{-3} we infer from Table 16. At $z \sim 0.9$, the comparison is also very good, 13.1×10^{34} W Mpc^{-3} for the CFRS versus 9.2×10^{34} W Mpc^{-3} for the total rest-frame B luminosity. Comparisons of the total rest-frame B luminosity for our $\mathscr{E}$ galaxy spectral class with the CFRS "blue" galaxies are also very good. This is quite encouraging and suggests that fundamentally our sample and the CFRS are in good agreement to $z \sim 0.9$, but the different analysis procedures, sample sizes, sample uncertainties, etc., have led in some cases to quite different values determined for α and L^* between the two projects.

Im et al. (2001) have analyzed the LF for a sample of 145 red field E/S0 galaxies selected through their morphology on deep *HST* images and their colors to have $16.5 < I < 22$ and expected to be at $z \lesssim 1$. Of these, 44 have spectroscopic redshifts, with photometric redshifts being used for the remaining galaxies. Their analysis is similar in many ways to ours; for example, in their preferred method, they fix α with redshift to -1.0, a somewhat steeper faint-end slope than that we find for early-type galaxies. They find a brightening in rest-frame B of 1.1–1.9 mag between $z = 0$ and 0.8, which is in good agreement with our result. Their constraint on the variation of number density with redshift (constant to within a factor of 2 between $z = 0$ and 0.8) is considerably looser than our constraint developed in § 7.

11.4. *Comparison with Previous Results at $z \sim 3$*

Steidel et al. (1999) give an analysis of the LF for $z \sim 3$ Lyman break galaxies. Since theirs is a photometrically selected sample, with spectroscopic confirmation of only a fraction of these, they reach about as deep into the LF at $z \sim 3$ as we do in our highest redshift bins. They find $\alpha = -1.60 \pm 0.13$, with a UV luminosity density which when converted into the units used here and with a correction factor applied for carrying the integration as faint as $L^*/20$ becomes $\rho(L)$ at 1500 Å of 1.1×10^{34} W Mpc^{-3}. This value is within a factor of 2 of the value we find for $\rho(L)$ at 2400 Å at $z \sim 1$. The comoving number density they derive for Lyman break galaxies at $z \sim 3$ (i.e., their value of ϕ^*) is very close to our value for $\mathscr{A}$ galaxies and smaller by a factor of ~ 5 than that for our total sample.

Steidel et al. (1999) find a value of $\log [L^*(W)]$ at 1500 Å of 37.59 dex. Our value at 2400 Å for galaxies at $z \sim 1.2$ is almost a factor of 10 smaller, but when extrapolated to their very steep faint-end slope, we find $\log [L^*(2400\ \text{Å})(W)] \sim 37.15$ dex, only a factor of ~ 3 smaller.

12. COMPARISON OF LUMINOSITY EVOLUTION DETERMINED THROUGH OTHER METHODS

There are a number of other methods of determining the evolution of luminosity with redshift. Studies of the fundamental plane of elliptical galaxies by Pahre, Djorgovski, & de Cavallho (1998) and Jorgenson et al. (1999) have determined with considerable precision the location of the fundamental plane for nearby galaxies in the field and in nearby rich clusters. Kelson et al. (2000) and van Dokkum et al. (1998) have explored rich clusters with deep *HST* imaging (CL 1358+62 with $z = 0.33$ and MS 1054−3 with $z = 0.83$) to analyze the evolution of early-type galaxies, finding that for rest-frame B $M/L_B \propto (-1.0 \pm 0.1)z$. This value should be compared to that we obtain for quiescent galaxies, $Q = 0.65$ (with a large uncertainty), which corresponds to -1.6 mag.

Kochanek et al. (2000) have used the properties of a small sample of gravitational lenses as determined from *HST* images and from mass models of the systems (used to estimate the central velocity dispersion of the galaxy) to constrain the evolution of the fundamental plane of field elliptical galaxies. They demonstrate that to within the uncertainties of their analysis the lens galaxies appear to behave similarly to the cluster elliptical galaxies.

For spiral galaxies, the Tully-Fisher relation provides a way of determining galaxy masses. Here the high-redshift galaxies have been attempted with the Low Resolution Imaging Spectrometer (LRIS) at Keck by Vogt et al. (1996, 1997), who have succeeded in measuring optical rotation curves for a small sample of $0.1 < z < 0.8$ galaxies with emission in the [O II] line at 3727 Å. They find only a small offset of ≤ 0.4 mag in rest-frame B with respect to the local relation, which they ascribe to luminosity evolution in the field galaxy sample. This value is consistent with the modest

values of Q found for star-forming galaxies in the present analysis.

There have been a number of attempts to study the LF in the HDF using photometric redshifts, including the work of Sawicki, Lin, & Yee (1997), Connolly et al. (1997), and Pascarelle, Lanzetta, & Fernandez-Soto (1998), as well as the NICMOS-based studies of Thompson, Weymann, & Storrie-Lombardi (2001) and Dickinson (2001). The area on the sky of the HDF is very small, and hence only a broad brush picture can thus be derived without insurmountable problems of small number statistics. Since the number of galaxies brighter than $R = 24$ is very small (~ 100) and essentially all of them have spectroscopic redshifts now, such efforts are most valuable as a means of exploring the regime beyond $z = 1.1$, where our sample is small, as well as the redshift "desert" between $1.5 < z < 2$ (once suitable calibration of the photometric redshifts exists there).

13. SUMMARY

This study of the LF of galaxies in the region of the HDF-N relies on the large databases built up in earlier papers in this series. It has been made feasible by the joining of the very complete redshift survey in that region of C00, the photometric catalogs of H00, and the rest-frame SED analysis of Cohen (2001). We divide the sample into six galaxy spectral class groupings, not all of which are independent, and five redshift bins. We use this data to carry out a classical LF analysis assuming that the Schechter function with fixed L^* and α is an adequate description within each redshift bin and for each galaxy spectral class grouping. We evaluate the LF at rest-frame 2400 Å, U, R, and K.

We find that the behavior of the faint-end slope is consistent with that observed in the local universe. The LFs for quiescent galaxies have shallow faint-end slopes, while those of galaxies with detectable emission lines have steeper faint-end slopes. Furthermore, as shown in Table 11 these slopes are independent of redshift out to $z = 1.05$ for each galaxy spectral grouping and agree well with comparable local determinations. The faint-end slopes are the same for rest-frame U, R, and K for each galaxy spectral grouping.

We assume that galaxy LFs for a particular galaxy spectral grouping and rest-frame wavelength change with redshift only through variations in L^* (and ϕ^*). We fix α, choosing a mean value from the set of full two-parameter LF fits, to obtain values of L^* for each galaxy spectral grouping in each of the redshift bins. We find that $\mathscr{A}$ galaxies become brighter with z with $Q \sim 0.6$ at all rest-frame bands studied here, where $Q = \Delta \log [L^*(z)]/\Delta z$, while galaxies with detectable emission lines (i.e., star-forming galaxies), which dominate the total sample, show a smaller change in L^* with redshift at all bands, $Q \sim 0.3$, becoming larger only at 2400 Å.

Passive evolution models of galaxies are in reasonable agreement with these results for absorption-line–dominated galaxies, while plausible star formation histories can reproduce the behavior of the emission-line galaxies. The major discrepancy with the specific set of galaxy spectral synthesis models we adopt, those of Poggianti (1997), is the prediction of much more luminosity evolution at rest-frame U for galaxies with a brief single initial burst of star formation than is actually inferred from our analysis of quiescent galaxies. This problem appears to be eliminated when Poggianti's very recent unpublished (B. M. Poggianti 2001, private communication) models are used.

Our naive view as illustrated in Figure 14 of C00 of the $z \gtrsim 1$ universe is one sparsely populated with bright blue galaxies, but we now see that this is too simplistic. The comoving number density of $\mathscr{A}$ galaxies drops rapidly beyond $z = 0.8$, but the SED analysis shows clearly that this is due to them becoming EROs which are too faint to be included in our R-selected sample. Correcting for this, the comoving number density appears to be roughly constant for each of the various galaxy spectral groupings, until the highest redshift bin is reached. There, for $1.05 < z < 1.5$, the apparent number density is a factor of ~ 10 low at all bands. We correct for selection effects resulting from the variation of our ability to determine redshifts as a function of z itself by throwing all galaxies without redshifts within the magnitude cutoffs of the sample into the highest z bin. We also make a generous allowance for galaxies near the faint end of the sample that are missing from the ground-based photometric catalogs. These, with several other smaller factors, are just barely sufficient when applied at their maximum possible values to allow constant comoving number density from $z = 0.25$ to 1.5, with considerable uncertainty at the highest redshift range. If less extreme correction factors are used, the comoving number density of luminous galaxies begins to decline at $z > 1$.

We calculate comoving luminosity densities. We find that the contributions to the total change as one would expect. $\mathscr{A}$ galaxies, being redder, contribute a larger fraction of the luminosity density at longer rest-frame wavelengths. We then use galaxy evolution models to extrapolate back to $z = 0.0$ the comoving luminosity densities at K for each redshift bin (see Table 17). From this, we can then calculate the total stellar mass in galaxies which appears to be constant to within 15% over this redshift range. We confirm that the UV luminosity density, an indicator of star formation, increased by a factor of ~ 4 over the period $z = 0$–1.

We find the comoving number density and the stellar mass in galaxies to be approximately constant out to $z \sim 1.05$, and with more uncertainty, to $z \sim 1.3$. The major epoch(s) of star formation and of galaxy formation must have occurred even earlier.

An examination of alternate possibilities for the assumptions made here shows that while the values of the LF parameters themselves (i.e., α and L^*) may depend on the detailed assumptions made in the analysis, parameters involving integration over the LF, such as the luminosity density, are robust.

In spite of our best efforts, and with a total sample of 735 objects with redshifts in this field, the numbers of galaxies are still small in the highest redshift bin considered here with $1.05 < z < 1.5$. To attempt a fainter magnitude limited survey with existing telescopes and instrumentation would be extremely expensive in terms of observing time. Our plans for future work to extend and reinforce these results will concentrate on targeted surveys guided by photometric criteria for candidate selection.

The entire Keck/LRIS user community owes a huge debt to Jerry Nelson, Gerry Smith, Bev Oke, and many other people who have worked to make the Keck Telescope and LRIS a reality. We are grateful to the W. M. Keck Foundation, and particularly its late president, Howard Keck, for the vision to fund the construction of the W. M. Keck

Observatory. We thank Roger Blandford and George Efstathiou for helpful discussions. We thank Amy Barger and Len Cowie for access to their unpublished photometric database for the region of the HDF. We thank the referee for constructive and helpful suggestions. This work was not supported by any federal agency.

APPENDIX A

SED PARAMETERS FOR SIX GALAXIES FROM DAWSON ET AL. (2001)

We give the SED parameters for six galaxies in the Flanking Fields from the 12 new redshifts from Dawson et al. (2001). (The other six are fainter than the cutoffs adopted here.) Five of these are in the *R*-selected sample; all are in the *K*-selected sample. Based on the description of their spectra given by Dawson et al. (2001), five are *&* galaxies while F36398_1602 is assigned a galaxy spectral class of *A*. The sBB SED model was used to derive the parameters given in Table 19.

TABLE 19

SED Parameters for Additional Galaxies in the Flanking Fields of the HDF

R.A.	Decl.[a]	z[a]	log [$L(\lambda_m$:blue] (W)	α_{UV} (sBB)	log [$L(\lambda_m$:red] (W)	T (K)
−12 36 22.07.....	−62 14 59.7	0.849	36.29	0.89	36.37	9155
−12 36 24.16.....	−62 15 14.4	0.796	36.39	1.72	36.42	15470
−12 36 25.52.....	−62 15 10.7	0.680	36.04	2.21	36.20	5305
−12 36 33.99.....	−62 16 04.6	0.834	36.58	1.08	36.64	6440
−12 36 39.82.....	−62 16 01.3	0.843	36.61	10.00	36.57	4825
−12 36 45.24.....	−62 11 08.7	0.512	35.59	−0.27	35.73	8300

Note.—Units of right ascension are hours, minutes, and seconds, and units of declination are degrees, arcminutes, and arcseconds.

[a] From Dawson et al. 2001.

APPENDIX B

AN ALTERNATIVE DERIVATION OF THE LUMINOSITY DENSITY

Because of our small sample size and wide redshift range, we needed to make several simplifying assumptions to achieve a satisfactory LF analysis of our data. In the main body of this paper, we followed conventional ideas about the anticipated evolution of the LF, assuming that α remains fixed with redshift while L^* changes. Note that this does not amount to assuming pure luminosity evolution, as ϕ^* is determined from the data and the number density is never constrained to be constant with redshift.

In this appendix, at the suggestion of the referee, we explore the opposite extreme assumption. We assume that $L^*(R)$ is fixed with redshift and that α may vary with z. In this case, unlike in the former, the values of ϕ^* for a specified galaxy spectral grouping in the various redshift bins cannot be intercompared to yield the relative number density of galaxies. Furthermore, any discussion of the evolution of L^* with redshift is meaningless, as L^* is fixed.

We calculate the luminosity density, which we expect to be the most robust parameter in our analysis, as it, together with the total number of galaxies per unit volume brighter than some specified cutoff, represents integrals over the LF. The results for the modified assumptions are given in Table 20. We compare $\rho(L)$ with the luminosity densities at rest-frame R given in Table 16. The comparison is very good; the two values of $\rho(L)$ agree to within 20% over the entire redshift range for each of the six galaxy spectral groups. Since these represent the extreme opposite assumptions that can be made in the LF analysis, we conclude that the determination of luminosity densities is very robust, as expected.

We expect both solutions discussed here, that with α fixed given in the main body of this paper or that with L^* fixed as given in this appendix, to be satisfactory fits to the data. We consider next whether there is any way we can judge which of these two is more likely to be valid. The banana-shaped error contours in the two-dimensional space with axes α, L^* (see Figs. 1–6) form the basis for our treatment. We proceed to diagonalize the covariance matrix by defining a new coordinate system which follows the long major axis of the banana-shaped error contours with a second axis perpendicular to that. We measure the difference between the constrained solution obtained by fixing α or alternatively L^* (i.e., the solutions given in Tables 5 and

TABLE 20

REST-FRAME R LF SOLUTION FOR FIXED L^* FOR EACH GALAXY SPECTRAL GROUPING

z Range	Total Number[a]	log [$L^*(R)$] (log W) (fixed)	α	ϕ^* (Mpc^{-3})	$\rho[L(R)]$ (10^{34} W Mpc^{-3})
		$\mathscr{A}$ Galaxies			
0.25–0.5.....	17	37.24	−0.78	0.0018	1.4
0.5–0.8	36	37.24	−0.50	0.0033	2.8
0.8–1.05.....	19	37.24	−0.08	0.0022	2.0
		$\mathscr{I}$ Galaxies			
0.25–0.5.....	62	36.86	−0.37	0.116	4.3
0.5–0.8	63	36.86	−0.05	0.0066	3.1
0.8–1.05.....	14	...	...	...	...
		$\mathscr{A}$ + $\mathscr{I}$ Galaxies			
0.25–0.5.....	79	37.02	−0.55	0.012	6.0
0.5–0.8	99	37.02	−0.20	0.011	5.8
0.8–1.05.....	33	37.02	+0.63	0.0032	3.3
		$\mathscr{I}$ + $\mathscr{E}$ Galaxies			
0.25–0.5.....	131	37.15	−1.27	0.0073	5.7
0.5–0.8	164	37.15	−1.25	0.0066	5.1
0.8–1.05.....	125	37.15	−1.35	0.0108	8.9
		$\mathscr{E}$ Galaxies			
0.25–0.5.....	69	36.85	−1.55	0.0040	1.9
0.5–0.8	101	36.85	−1.45	0.0052	2.3
0.8–1.05.....	111	36.85	−0.82	0.02 1	7.3
		All Galaxies			
0.25–0.5.....	148	37.43	−1.33	0.0051	7.9
0.5–0.8	200	37.43	−1.25	0.0049	7.6
0.8–1.05.....	144	37.43	−1.45	0.0066	11.1

[a] The numbers of galaxies in the HDF and in the Flanking Fields, respectively, can be found from Table 5.

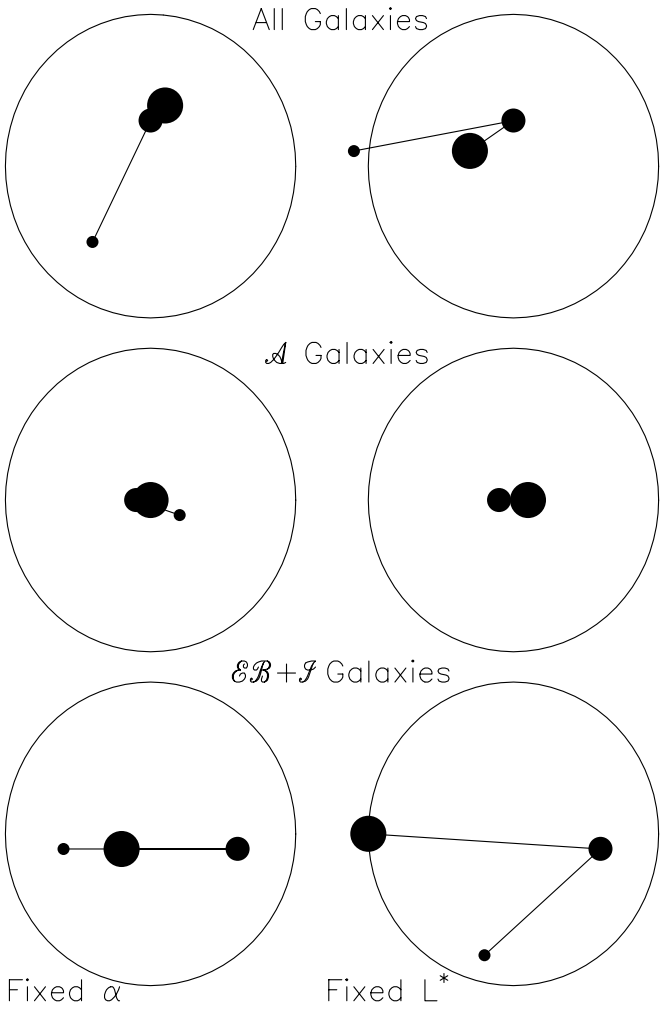

FIG. 13.—Diagonalized errors shown for the two different assumptions adopted here in the LF solution. On the left side are those obtained when α is fixed as a function of redshift for each galaxy spectral grouping. On the right side, those given in Appendix B, where L^* is maintained fixed instead, are displayed. The difference between the (α, L^*) found in these solutions and the values found with the full two-parameter solutions of § 3.1 is expressed in units of 1 σ rms deviations. The large circles denote a total rms difference of 1 σ. The results are shown for three redshift bins $0.25 < z < 0.5$, $0.5 < z < 0.8$, and $0.8 < z < 1.05$, as well as for three galaxy spectral groupings. The symbol size increases as the mean redshift of the bin increases. See text for details.

20) and the full two-parameter solution given in Table 3 in units of σ. To accomplish this, we examine each of the error contours in the α-L^* plane and measure σ_l and σ_s in these "long" and "short" coordinates.

Figure 13 presents the results for rest-frame R. The large circles represent 1 σ rms difference. The horizontal axis is σ_l, while the vertical axis is σ_s. Three redshift bins were used, $0.25 < z < 0.5$, $0.5 < z < 0.8$, and $0.8 < z < 1.05$, for each of three galaxy spectral groupings. The galaxy spectral groupings used are all galaxies, $\mathscr{A}$ galaxies, and $\mathscr{E} + \mathscr{I}$ galaxies. The latter two are chosen as they are believed to be the pair which sum to the whole sample and which are most likely to be stable in terms of technical problems over the range of redshift considered here (see §§ 3.1 and 6.2). On the left side of the figure are the differences for the solution where α is fixed, while on the right are the solutions for the case in which L^* is held fixed.

We see that both of these assumptions lead to reasonably good solutions, lying within a difference of less than 1 σ (i.e., within the large circles) in most cases. For the $\mathscr{A}$ galaxies, where the sample is very small and the errors are quite large (see Tables 5 and 20 for the corresponding uncertainties in the α-L^* plane), little distinction is possible. However, when one looks at the other two spectral classes presented in this figure, where the samples are much larger, the solution with fixed L^* has slightly larger deviations (appearing as a larger mean distance of the points from the center of the circle) than does the solution with fixed α. We therefore can have at least some degree of confidence that luminosity evolution is in fact occurring in our sample. Only with a larger, deeper, better sample will we be able to refine this analysis and this potential discriminant.

REFERENCES

Barger, A. J., Cowie, L. L., Trentham, N., Fulton, E., Hu, E. M., Songaila, A., & Hall, D. 1999, AJ, 117, 102
Bertin, E., & Arnouts, S. 1996, A&AS, 117, 393
Blanton, M. R., et al. 2001, AJ, 121, 2358
Cohen, J. G. 2001, AJ, 121, 2895
Cohen, J. G., Hogg, D. W., Blandford, R., Cowie, L. L., Hu, E., Songaila, A., Shopbell, P., & Richberg, K. 2000, ApJ, 538, 29 (C00)
Cohen, J. G., Hogg, D. W., Pahre, M. A., Blandford, R., Shopbell, P. L., & Richberg, K. 1999, ApJS, 120, 171
Cole, S., et al. 2001, MNRAS, 326, 255
Connelly, A. J., Szalay, A. S., Dickinson, M., SubbaRao, M. U., & Brunner, R. J. 1997, ApJ, 486, L11
Cowie, L. L., Songaila, A., & Barger, A. J. 1999, AJ, 118, 603
Cross, N., et al. 2001, MNRAS, 324, 825
Daddi, E., Cimitti, A., & Renzini, A. 2000, A&A, 362, L45
Dawson, S., Stern, D., Bunker, A. J., Spinrad, H., & Dey, A. 2001, AJ, 122, 598
de Bernardis, P., et al. 2000, Nature, 404, 955
Dickinson, M. 2001, in Building Galaxies: From the Primordial Universe to the Present, Moriond Astrophysics Meeting (1999 March), ed. F. Hammer et al. (Paris: Editions Frontieres), 257
Driver, S. 2001, in Deep Fields, ed. S. Cristiani, A. Renzini, & R. E. Williams (Berlin: Springer), 86
Efstathiou, G., Ellis, R. S., & Peterson, B. P. 1988, MNRAS, 232, 431
Fernandez-Soto, A., Lanzetta, K. M., & Yahil, A. 1999, ApJ, 513, 34
Folkes, S., et al. 1999, MNRAS, 308, 459
Fukugita, M., Ichikawa, T., Gunn, J. E., Doi, M., Shimasaku, K., & Schneider, D. P. 1996, AJ, 111, 1748
Hogg, D. W., Cohen, J. G., Blandford, R., & Pahre M. A. 1998, ApJ, 504, 622
Hogg, D. W., et al. 2000, ApJS, 127, 1 (H00)
Im, M., et al. 2001, ApJ, submitted
Jorgenson, I., Franx, M., Hjorth, J., & van Dokkum, P. G. 1999, MNRAS, 308, 833
Kelson, D. D., Illingworth, G. D., van Dokkum, P. G., & Franx, M. 2000, ApJ, 531, 184
Kennicut, R. C. 1998, ARA&A, 36, 189
Kochanek, C. S., et al. 2000, ApJ, 543, 131
———. 2001, ApJ, 560, 566
Le Févre, O., Crampton, D., Lilly, S. J., Hammer, F., & Tresse, L. 1995, ApJ, 455, 60
Lilly, S. J., Le Fèvre, O., Hammer, F., & Crampton, D. C. 1996, ApJ, 460, L1
Lilly, S. J., Tresse, L., Hammer, F., Crampton, D., & Le Fèvre, O. 1995, ApJ, 455, 108
Lin, H., Kirshner, R. P., Shectman, S. A., Landy, S. D., Oemler, A., Tucker, D. L., & Schechter, P. L. 1996, ApJ, 464, 60
Lin, H., Yee, H. K. C., Carlberg, R. G., Morris, S. L., Sawicki, M., Patton, D. R., Wirth, G., & Shepherd, C. W. 1999, ApJ, 518, 533
Marzke, R. O., Huchra, J. P., Huchra, J. P., & Corwin, H. G. 1994, AJ, 108, 437
Pahre, M. A., Djorgovski, S. G., & de Carvalho, R. R. 1998, AJ, 116, 1606
Pascarelle, S. M., Lanzetta, K. M., & Fernandez-Soto, A. 1998, ApJ, 508, L1
Petrosian, V. 1976, ApJ, 209, L1
Poggianti, B. M. 1997, A&AS, 122, 399
Press, W. H., Flannery, B. P., Teukolsky, S. A., & Vetterline, W. T. 1986, Numerical Recipes in Fortran (Cambridge: Cambridge Univ. Press)
Sandage, A. R., Tammann, G. A., & Yahil, A. 1979, ApJ, 232, 352
Sawicki, M., Lin, H., & Yee, H. K. C. 1997, AJ, 113, 1
Schechter, P. L. 1976, ApJ, 203, 297
Shectman, S. A., Landy, S. D., Oemler, A., Tucker, D. L., Lin, H., Kirshner, R. P., & Schechter, P. L. 1996, ApJ, 470, 172
Skrutskie, M. F., et al. 1997, in The Impact of Large Scale Near-IR Surveys, ed. F. Garzon et al. (Dordrecht: Kluwer), 187
Steidel, C. C., Adelberger, K. L., Giavalisco, M., Dickinson, M., & Pettini, M. 1999, ApJ, 519, 1
Thompson, D., et al. 1999, ApJ, 523, 100
Thompson, R., Weymann, R. J., & Storrie-Lombardi, L. J. 2001, ApJ, 546, 694
Treyer, M. A., Ellis, R. S., Milliard, B., & Bridges, T. J. 1998, MNRAS, 300, 303
van Dokkum, P. G., Franx, M., Kelson, D. D., & Illingworth, G. D. 1998, ApJ, 504, L17
Vogt, N. P., et al. 1997, ApJ, 479, L121
Vogt, N. P., Forbes, D. A., Phillips, A. C., Gronwall, C., Faber, S. M., Illingworth, G. D., & Koo, D. C. 1996, ApJ, 465, L15
Williams, R. E., et al. 1996, AJ, 112, 1335
Yee, H. K. C., et al. 2000, ApJS, 129, 475